High-order Sparse-PIC methods: analysis and numerical investigations

Fabrice Deluzet, Clément Guillet, Jacek Narski, Paul Pace

High-order Sparse-PIC methods: analysis and numerical investigations

Fabrice Deluzet[†] Clément Guillet[†*] Jacek Narski[†]
Paul Pace[†]

[†]Université de Toulouse; UPS, INSA, UT1, UTM,
Institut de Mathématiques de Toulouse,
CNRS, Institut de Mathématiques de Toulouse UMR 5219,
F-31062 Toulouse, France,

February 4, 2024

Abstract

Particle-In-Cell (PIC) methods embedding Sparse grids have been recently introduced to decrease the statistical noise inherent to PIC approximations. In Sparse-PIC methods, the numerical noise is filtered out from the approximation thanks to a reconstruction of the grid quantities on a hierarchy of coarse meshes. This procedure introduces a significant gain in the precision of the numerical approximation with respect to the mean number of particles in a grid cell, this parameter controlling the numerical noise, but, also a slight discrepancy of the method precision with respect to the mesh resolution. In precedent studies, this issue is addressed by a careful tuning of the sparse grids composing the grid hierarchy, to define a trade-off between the gain in the numerical noise and the loss in the grid resolution. The present work is dedicated to improving the precision of Sparse-PIC methods with respect to the mesh resolution and, contrary the precedent achievements, without deriorating the gains with respect to the statistical noise.

1 Introduction

Particle-In-Cell (PIC) methods have been popular for plasma physics simulations since the early interest for the discretization of kinetic plasma models [1, 18, 5]. These numerical methods stand out due to their Eulerian-Lagrangian nature, the distribution function accounting for the plasma properties being sampled by a set of numerical particles while Maxwell's equations governing the changes in the electromagnetic field are discretized by Finite Differences (or Finite Elements) on a mesh. These two sets of equations are coupled, first by means of the source terms of the field equations, namely the charge and current densities defined by the moments of the distribution function and, second, through the electric forces defining the acceleration experienced by the particles. The properties of the numerical particles are therefore projected onto the mesh making possible the computation of the field on the mesh. It is interpolated onto the particle position to integrate the particles trajectories discretizing by this means the evolution of the distribution function.

Compared to Eulerian discretizations, PIC methods offer a significant gain in computational efficiency. Indeed, the distribution function is a function of the phase space which may be three-dimensional for the spacial variable and also three-dimensional for the kinetic velocity, yielding a problem with six dimensions plus time. In PIC methods, the Lagrangian discretization of the kinetic equation offers a linear complexity with respect to the dimensionality of the problem, which shall be

*Corresponding author
clement.guillet@math.univ-toulouse.fr

compared to the exponential complexity of Eulerian discretizations. On top of that, PIC methods are quite simple to implement, eventually the analogy between the numerical particles and the real ones permits easy insights into the physics described by the system.

Nonetheless, the sampling of the distribution function by a limited number of particles introduces a statistical noise on the quantities deposited onto the grid for the computations of the field. The precision of the approximation of the distribution function moments may be analyzed thanks to a decomposition of the error between the continuous quantity and the statistical estimator, issued from the particle sampling, into two components. The first one is the grid based error. It characterizes the precision with which a moment of the distribution function is approximated by the most probable value of the statistical estimator. This component of the error is controlled by the mesh size of the grid as well as the smoothness of the approximated quantity. The second part of the error is the variance of the statistical estimator. This component of the error decreases slowly with the number of numerical particles, precisely with the square rout of the mean number of particles per grid cell. This very low convergence rate explains why, in most computations, the statistical noise is the most detrimental component of the error, the increase in the number of particles being necessarily massive to obtain a meaningful improvement in the numerical noise.

Huge efforts have been devoted to the development of noise reduction strategies for PIC methods. The δf [9, 23] and micro-macro methods operate a decomposition of the distribution function into a Maxwellian part complemented with a correction. The parameters of the Maxwellian are evolved thanks two a fluid like system, while the remaining correction is discretized thanks to particles. The gain here are significant when the distribution function remains a moderate perturbation of a Maxwellian. Other approaches are conceived like a post-processing of the procedure defining distribution function moments onto the mesh and the interpolated field onto the particles position by means of quadratic or Fourier ou wavelets [14] filtering.

The Sparse-PIC methods enters this class of noise reduction strategies insofar as the projection of the distribution moments as well as the interpolation of the field are modified to provide a better control of the numerical noise. This method has been introduced first by Ricketson et al. [21, 20]. It relies on a substitution of the Cartesian mesh with a hierarchy of sparse grids referred to as component grids. The combination technique provides the definition of an interpolant reconstructed from the data deposited onto each of the component grids. Both the component grids populating the grid hierarchy and the coefficients involved in the combination procedure are selected to cancel the approximation errors originating from the grids with the coarsest resolutions, yielding a recombined interpolant with a grid based error only marginally deteriorated compared to that of the moment projected onto the Cartesian grid classically operated in regular PIC methods. The main advantage of Sparse-PIC methods comes from the fact that the component grids are very sparse, composed of an extremely reduced number of anisotropic cells with a coarse resolution at least in one direction. This characteristic increases the number of mean particles contains in the cells of each of this component grids which entails a damping of the numerical noise [6]. Sparse-PIC methods have been applied to the classical benchmarks of kinetic plasma physics (*e.g.* the simulation of the Landau damping and diocotron instability) then conclusively extended to the simulations of low temperature (and collisional) plasma discharge as well as drift instabilities in Hall plasma thrusters [13, 12, 11]. Then semi-implicit formulation of the method [17] have been investigated, as well as the efficiency of the method for three-dimensional computations on either shared memory CPU [7] or GPU [8]. These last developments have demonstrated the interesting property of the method with respect to the noise control and outline that, for specific applications, the deterioration of the grid based error may be detrimental to the quality of the approximation. So far, this issue has been addressed by means of the so-called truncated [21, 20] and offset [6] technics. They boils down mainly to tuning the choice of the component grids populating the sparse grid hierarchy in order to balance the gains in the statistical noise mitigation and the loss related to the grid based error. In other words, the improvements obtained on the grid based error comes necessarily with a deterioration of the statistical noise damping.

The aim of the present work is to address this same issue but through the introduction of high-order Spars-PIC methods. The existing Sparse-PIC methods are limited to second order discretizations, while the methods introduced herein offer fourth to sixth order space discretizations. The precision of these high-order Sparse-PIC methods is analyzed and proved to bring gains on the grid based error without deteriorating the noise damping.

The paper is organized into three sections. Sec. 2 is devoted to the introduction of the continuous model at hand for the present work, namely the Vlasov-Poisson system. The principles of Particle-In-Cell methods are then briefly exposed before introducing the Sparse-PIC methods together with the so-called "Offset" technic introduced to mitigate the deterioration of the grid based error. An

overview of the error estimates for all these methods in proposed to highlights the strengths and the weaknesses of each of them. Sec. 3 is devoted to the development and analysis of high-order Sparse-PIC methods. Estimates for the grid based error as well as the numerical noise are derived highlighting that, provided the solution is smooth enough, the gird based error may be improved without ay deterioration of the statistical noise compared to second Sparse-PIC methods. Numerical investigations are conducted within Sec. 4 outlining the improvements brought by the high-order space discretization.

2 PIC and Sparse-PIC methods for Plasma Simulation

2.1 The Vlasov-Poisson Model

Cold plasma simulations find their anchor in the Vlasov-Poisson equations, which provide an essential tool for unraveling the collective dynamics of charged particles in a collision-less environment. The set of equations writes

$$\partial_t f_s + \mathbf{v}\cdot\nabla_{\mathbf{x}} f_s + \frac{q_s}{m_s}(\mathbf{E}+\mathbf{v}\times\mathbf{B})\cdot\nabla_{\mathbf{v}} f_s = 0 \tag{1a}$$

where $f_s(\mathbf{x},\mathbf{v},t)$ is the distribution function attached to the electrons ($s=e$) of the ions ($s=i$) of charge q_s and mass m_s. These functions depend on the space variable $\mathbf{x}\in\Omega_x\subset\mathbb{R}^{d_x}$ and the velocity $\mathbf{v}\in\Omega_v\subset\mathbb{R}^{d_v}$, d_x+d_v being the dimension of the phase space $\Omega_x\times\Omega_v$, and $t\in\mathbb{R}^+$ the time. In the following we use $d=d_x$ for ease of notation.

In the present work, the magnetic field, denoted $\mathbf{B}$, is assumed to be time independent, the electric field $\mathbf{E}$ being therefore electrostatic, deriving from a potential ϕ solution to the Poisson equation:

$$-\Delta\phi = \frac{\rho}{\epsilon_0}\,, \qquad \mathbf{E} = -\nabla\phi\,. \tag{1b}$$

The source term of the Poisson equation (1b) is the ratio of the charge density ρ and ϵ_0 the vacuum permittivity. The charge density is defined thanks to the moment of the distribution functions

$$\rho(\mathbf{x},t) = \sum_s q_s \int_{\Omega_v} f_s(\mathbf{x},\mathbf{v},t)d\mathbf{v} \tag{1c}$$

To simplify the framework, the ions will generally be considered motion-less in the next sections, the only evolution of the electrons being accounted for by the system. Accordingly, the subscript s will be dropped from the notations, the distribution function f being related to electrons. The time dependence of the quantity will also be omitted to simplify the notations.

2.2 The PIC method

The idea that ties the Particle-In-Cell method is to merge two discretization methods: an Eulerian discretization of the field equations coupled to a Lagrangian of the kinetic equations. The Poisson equation will be discretized by Finite Difference on a Cartesian grid, denoted Ω_{h_n}, h_n is the mesh step assumed to uniform in any direction. Assuming a periodic domain, the grid nodes are defined as

$$\mathbf{x}_{\mathbf{j}} = \mathbf{j}\cdot h_n\,, \quad \mathbf{j}\in\mathbf{I}_{h_n} := \bigotimes_{i=1}^{d} [\![0, 2^n-1]\!]\,, \qquad h_n = 2^{-n}\,. \tag{2}$$

In these definitions, $\mathbf{I}_{h_n}$ is a set of multi-indices $\mathbf{j}$ and $\mathbf{x}_{\mathbf{j}} = (\mathbf{x}_{j_1,\dots,j_d})$, $j_i\in[\![0,2^n-1]\!]$, for $1\le i\le d$ are the coordinate vectors of the grid nodes.

Denoting $\mathcal{Q}$ the total charge related to one specie, the charge density defined by Eq. (1c) may be recast into

$$\rho(\mathbf{x}) = \mathcal{Q}\iint_{\Omega_v\times\Omega_x} \delta(\boldsymbol{\xi}-\mathbf{x}) f(\boldsymbol{\xi},\mathbf{v})d\mathbf{v}d\boldsymbol{\xi}\,. \tag{3}$$

An approximation of this quantity is obtained by substituting the Dirac distribution by a shape function W_{h_n} related to the mesh size. For d-dimensional problem, W_{h_n} is constructed as a tensor

product of a one-dimension function:

$$W_{h_n}(\mathbf{x}) = \bigotimes_{i=1}^{d} W_{h_n}(x_i)\,, \qquad w_{h_n}(x_i) = h_n^{-1} W(h_n^{-1} x_i)\,. \tag{4a}$$

The most popular choice of function for W, referred to as the "Cloud In Cell" function in the PIC literature, is denoted W^2 within this document. This is a piece-wise linear function defined as

$$W^2(x) = \begin{cases} 1 - |x| & \text{if } |x| \leq 1 \\ 0 & \text{otherwise.} \end{cases} \tag{4b}$$

This yields the following approximation of the charge density

$$\rho_{h_n}(\mathbf{x}) = \mathcal{Q} \iint_{\Omega_v \times \Omega_x} W_{h_n}(\boldsymbol{\xi} - \mathbf{x}) f(\boldsymbol{\xi}, \mathbf{v}) d\mathbf{v} d\boldsymbol{\xi}\,. \tag{5}$$

This integral is statistically sampled, following a Monte Carlo approximation (see [6, 22] for further developments), to obtain the statistical estimator of the density

$$\hat{\rho}_{h_n}(\mathbf{x}) = \mathcal{Q} \frac{1}{N} \sum_{p=1}^{N} W_{h_n}(\mathbf{x} - \mathbf{x}_p)\,, \tag{6}$$

where N is the number of random variables used to sample the integral, assimilated to the numerical particle positions $\mathbf{x}_p$, $1 \leq p \leq N$. To define a discretization of the Vlasov equation, the position and the velocity of the numerical particles $(\mathbf{x}_p(t), \mathbf{v}_p(t))$ obey the Newton laws

$$\frac{d}{dt}\mathbf{x}_p(t) = \mathbf{v}_p(t)\ , \qquad \frac{d}{dt}\mathbf{v}_p(t) = \frac{q}{m}\mathbf{E}\left(\mathbf{x}_p(t)\right)\ , \qquad 1 \leq p \leq N\,. \tag{7}$$

The different nature of the discretizations applied to either the field or the Vlasov equation calls for the introduction of an interpolation operator in order to define the electric field at the particles position. This yields the following definition.

Definition 2.1 *Let $W_{h_n;\mathbf{j}}$ be the shape functions centered on the grid nodes $\mathbf{x}_\mathbf{j}$ and V_{h_n} the space spanned by the functions $(W_{h_n;\mathbf{j}})_{\mathbf{j}\in\mathbf{I}_{h_n}}$*

$$W_{h_n;\mathbf{j}}(\mathbf{x}) := W_{h_n}(\mathbf{x}_\mathbf{j} - \mathbf{x})\,, \quad V_{h_n} := \operatorname*{span}_{\mathbf{j}\in\mathbf{I}_{h_n}}(W_{h_n;\mathbf{j}})\,, \tag{8}$$

the interpolant of the electric field is denoted $I_{V_{h_n}}(\mathbf{E}_{h_n})$ with

$$\mathcal{I}_{V_{h_n}}(\mathbf{E}_{h_n})(\mathbf{x}) := \sum_{\mathbf{j}\in\mathbf{I}_{h_n}} \mathbf{E}_\mathbf{j} W_{h_n;\mathbf{j}} \tag{9}$$

where $\mathbf{E}_{h_n} = (\mathbf{E}_\mathbf{j})_{\mathbf{j}\in\mathbf{I}_{h_n}}$ are the values of the electric field at the grid nodes.

Denoting Δ_{h_n} $\boldsymbol{\nabla}_{h_n}$, a classical leap-frog time discretization of the particle equations yields the four consecutive steps of the regular PIC method sketched by Alg. 1.

1. **Charge accumulation** onto the nodes $\mathbf{x_j}$, $\mathbf{j} \in \mathbf{I}_{h_n}$ of the grid Ω_{h_n} using the statistical estimator defined by Eq. (6)
2. **Field computation:**the finite differenced approximation of the electric field writes, for $\mathbf{j} \in \mathbf{I}_{h_n}$

$$-\left(\Delta_{h_n}\phi\right)_{\mathbf{j}} = \hat{\rho}^k_{h_n}(\mathbf{x_j})\,, \quad \mathbf{E}^k_{h_n}(\mathbf{x_j}) = -\left(\boldsymbol{\nabla}_{h_n}\phi\right)(\mathbf{x_j})\,. \tag{10}$$

3. **Field Interpolation:** Evaluate the electric field at the particles positions $\mathcal{I}_{V_{h_n}}(\mathbf{E}^k_{h_n})(\mathbf{x}^k_p)$ using the interpolant defined by Eq. (9).
4. **Integrate particles trajectories:** For $p = 1, \ldots, N$, k the time iteration,

$$\begin{aligned} \mathbf{v}_p^{k+1/2} &= \mathbf{v}_p^{k-1/2} + \Delta t \mathcal{I}_{V_{h_n}}(\mathbf{E}^k_{h_n})(\mathbf{x}^k_p)\,, \\ \mathbf{x}_p^{k+1} &= \mathbf{x}_p^k + \Delta t \mathbf{v}_p^{k+1/2}\,. \end{aligned} \tag{11}$$

Algorithm 1: Overview of the time step of a PIC method.

2.3 Sparse-PIC methods

2.3.1 Overview of the Sparse-PIC approximation

The idea behind Sparse methods is to focus on a collection of under-refined sub-grids in one direction instead of considering a single Cartesian grid; subsequently recombining them while canceling out errors in a telescopic manner. A detailed overview of Sparse methodology could be found in [16, 2, 10, 3]. The presentations of the Sparse-PIC method requires the introduction of specific tools to Sparse grids. This is the purpose of the next definitions.

First an order relation on the multi-indices is introduced. We introduce the multi-index partial order:

Definition 2.2 (Norm and oder relation on multi-indices) *Let* $\mathbf{k} = (k_1, \ldots, k_d)$ *and* $\mathbf{l} = (l_1, \ldots, l_d)$ *be two d-dimensional multi-indices, the following order relations and norm are defined*

$$\begin{aligned} &\mathbf{k} \leq \mathbf{l} \Longleftrightarrow k_i \leq l_i\,, \forall i \in \{1, \ldots d\} \\ &\mathbf{k} < \mathbf{l} \Longleftrightarrow \mathbf{k} \leq \mathbf{l} \text{ and } \exists i \in \{1, \ldots, d\} \mid k_i < l_i\,. \end{aligned} \tag{12}$$

The 1-norm of a multi index $\mathbf{l}$ *is*

$$\|\mathbf{l}\|_1 = \sum_{i=1}^{d} l_i \tag{13}$$

The component grids as well as the sparse grids may now be introduced.

Definition 2.3 (Component grid) *A d-dimensional component grid (or sub-grid) of level i is an anisotropic grid parameterized by a d-dimensional index* $\mathbf{l} \in \mathbb{L}_{n,i}$ *where*

$$\mathbb{L}_{n,i} := \{\mathbf{l} \in \mathbb{N}^d \mid \|\mathbf{l}\|_1 = n + d - 1 - i, \mathbf{l} \geq \mathbf{1}\},\ ; \tag{14a}$$

it is denoted $\Omega_{h_\mathbf{l}}$ *and defined by the set of nodes*

$$\Omega_{h_\mathbf{l}} := \{\mathbf{j}h_\mathbf{l} \mid \mathbf{j} \in \mathbf{I}_{h_\mathbf{l}}\} \subset \Omega, \quad \mathbf{I}_{h_\mathbf{l}} := [\![0, h_{l_1}^{-1}]\!] \times \ldots \times [\![0, h_{l_d}^{-1}]\!] \subset \mathbb{N}^d, \tag{14b}$$

where

$$h_\mathbf{l} := (h_{l_1}, \ldots, h_{l_d}) = 2^{-\mathbf{l}}, \qquad \mathbf{j}h_\mathbf{l} := (j_1 h_{l_1}, \ldots, j_d h_{l_d})\,. \tag{14c}$$

The parameter $h_\mathbf{l}$ *is referred to as the* ***grid discretization****.*

Definition 2.4 (Sparse grid) *A d-dimensional sparse grid is defined as a hierarchy of component grids with resolution levels i ranging from* 0 *to* $(d-1)$*. It is parameterized by the set of multi-indices*

$$\mathbb{L}_n := \bigcup_{i \in [0, d-1]} \mathbb{L}_{n,i}\,. \tag{14d}$$

The Cartesian grid Ω_{h_n} implemented in regular PIC methods together with the node index set $\mathbf{I}_{h_n}$ correspond to a sub-grid of level $\mathbf{n} = n \cdot \mathbf{1}_d$ yielding

$$\Omega_{h_n} := \{\mathbf{j}h_n \mid \mathbf{j} \in \mathbf{I}_{h_n}\} \subset \Omega, \quad \mathbf{I}_{h_n} := [\![0, h_n^{-1} - 1]\!]^d \subset \mathbb{N}^d$$

As mentioned previously, the essence of the Sparse-PIC methods is to substitute this Cartesian grid by sparse grid composed of a hierarchy of component-grids. It is therefore mandatory to extend the definition of the statistical estimator of the charge density onto a component grid and the interpolant of the electric field computed on a component grid.

Similarly to the regular PIC framework, the shape functions related to a component grid are constructed by tensor products of one-dimensional functions scaled with different grid steps along any dimension. This yields the definition

$$W_{h_\mathbf{l}}(\mathbf{x}) := \bigotimes_{i=1}^{d} W_{h_{l_i}}(x_i); \qquad W_{h_{l_i}}(x_i) = h_{l_i}^{-1} W(h_{l_i}^{-1} x_i)\,. \tag{15a}$$

Accordingly, the following estimator of the charge density projected onto a component grid $\Omega_{h_\mathbf{l}}$ is constructed:

$$\hat{\rho}_{h_\mathbf{l}}(\mathbf{x}) = \mathcal{Q}\frac{1}{N}\sum_{p=1}^{N} W_{h_\mathbf{l}}(\mathbf{x} - \mathbf{x}_p)\,. \tag{15b}$$

The interpolated electric field carried out on a sub-grid $\Omega_{h_\mathbf{l}}$ is defined similarly

$$\mathcal{I}_{V_{h_\mathbf{l}}}(\mathbf{E}_{h_\mathbf{l}}) = \sum_{\mathbf{j} \in \mathbf{I}_{h_\mathbf{l}}} \mathbf{E}_\mathbf{j} W_{h_\mathbf{l}}(\mathbf{x}_\mathbf{j} - \mathbf{x})\,, \quad \mathbf{E}_{h_\mathbf{l}} = (\mathbf{E}_\mathbf{j})_{\mathbf{j} \in \mathbf{I}_{h_\mathbf{l}}} \tag{15c}$$

The sparse-grid interpolants, related to the whole hierarchy of component grids, is constructed by combination of the interpolant issued from each component grid. To harvest a telescopic cancellation of the approximation errors, the recombined quantity are defined as follows [15, 6].

Definition 2.5 (Sparse grid surrogates) *The recombined electric field and particle density for the sparse grid parameterized by $\mathbb{L}_n = \cup_{i \in [0,d-1]} \mathbb{L}_{n,i}$, $\mathbb{L}_{n,i}$ being the set of component grids with a resolution level $\mathbb{L}_{n,i}$ as defined by Eq. (14a), are denoted $E^c_{h_n}$ and $\hat{\rho}^c_{h_n}$ and defined by*

$$E^c_{h_n}(\mathbf{x}) := \sum_{\mathbf{l} \in \mathbb{L}_n} c_\mathbf{l} \mathcal{I}_{V_{h_\mathbf{l}}}(E_{h_\mathbf{l}})(\mathbf{x})\,, \qquad \hat{\rho}^c_{h_n}(\mathbf{x}) := \sum_{\mathbf{l} \in \mathbb{L}_n} c_\mathbf{l} \mathcal{I}_{V_{h_\mathbf{l}}}(\hat{\rho}_{h_\mathbf{l}})(\mathbf{x})\,, \tag{16a}$$

the combination coefficients being, for any sub-grid $\Omega_{h_\mathbf{l}}$ of level i ($\mathbf{l} \in \mathbb{L}_{n,i}$),

$$c_\mathbf{l} := (-1)^i \frac{(d-1)!}{i!(d-1-i)!}\,. \tag{16b}$$

The steps of the Sparse-PIC method are very similar to that of the regular PIC methods, except that they are repeated on any of the component grids, for the charge density projection as well as electric field computation, then gathered (or recombined) on all the component grid to define the sparse grid interpolant used for the evaluation of the electric field at the particles position. This is outlined in Alg. 2.

1. **Charge accumulation** onto the nodes $\mathbf{x}_\mathbf{j}$, $\mathbf{j} \in \mathbf{I}_{h_\mathbf{l}}$ of the grid $\Omega_{h_\mathbf{l}}$ using the statistical estimator defined by Eq. (15b).
2. **Field computation** on any component grid $\Omega_{h_\mathbf{l}}$, $\mathbf{l} \in \mathbb{L}_n$ to obtain $\mathbf{E}_{h_\mathbf{l}}$ the finite difference approximation of the electric field.
3. **Field Interpolation:** Evaluate the recombined grid electric field at the particles positions $\mathbf{E}^{c,k}_{h_n}(\mathbf{x}^k_p)$ using the sparse grid interpolant defined by Eqs. (16).
4. **Integrate particles trajectories** using the local recombined electric field.

Algorithm 2: Overview of the time step of a Sparse-PIC method.

2.3.2 The Offset Sparse-PIC method

Sparse methods may be equipped with an additional pair of parameters to tune the grid selection embedded into the hierarchy defining the sparse grid surrogates [6]. To this end, the pair of parameters (τ^0, τ^1) is introduced with

$$(\tau^0, \tau^1) \in [\![1\ ,\ n]\!] \times [\![d-1\ ,\ (d-1)\tau^0]\!] \tag{17a}$$

where τ^0 is aimed at governing the minimum resolution level offered by the component grids. The second parameter, τ^1, is introduced to set the maximal resolution of the component grids. The definition of the resolution level i may now be written as

$$\mathbb{L}_{n,i}(\tau^0, \tau^1) := \{\mathbf{l} \in \mathbb{N}^d \mid \|\mathbf{l}\|_1 = n + \tau^1 - i, \mathbf{l} \geq \tau^0\} \tag{18}$$

Remark 2.6 *The definition of resolution level $L_{n,i}$ provided by Eq. (14a) is recovered setting $(\tau_0, \tau_1) = (1, d-1)$, $\mathbb{L}_{n,i} = \mathbb{L}_{n,i}(1, d-1)$, while the Cartesian grid implemented in regular PIC methods corresponds to the choice $(\tau_0, \tau_1) = (n, n)$.*

The offset addition to Sparse-PIC methods only alters the grid selection: all the steps defined in Alg. 2 are performed in the same manner but for a different set of grids.

Two parameters are instrumental to analyse the influence of the offset technique on the poperties of the Sparse-PIC methods:

$$n_1 = n - 2\tau_0 + \frac{\tau_1}{d-1}\,, \qquad n_2 = n + \tau_1 - (d-1)\,. \tag{19}$$

First, the modified definition of the resolution levels entails a reduces number of component grid defining the sparse grid hierarchy of the offset method $\mathcal{O}(\log(h_{n_1}))$ (compared to $\mathcal{O}(\log(h_n))$ for the non ofseted Sparse-PIC method) with $n_1 \leq n$. Second, the embedding of component grids with an increased resolution (sub-grids Ω_{h_1} with large $\|\mathbf{l}\|_1$) implies $n_2 \geq n$.

2.4 Error estimates

The PIC methods, by their hybrid nature, encompass aspects derived from both the Lagrangian and Eulerian worlds. To characterize the error incurred by the discretization, it is beneficial to decompose it into a component specific to the Monte Carlo method and a component including the grid dependencies.

Definition 2.7 *Denoting $\mathbb{E}(\hat{\rho})$ the expected value of a statistical estimator of the density, the local error between the density and this estimator may be recast into two components:*

$$\hat{\rho}(\mathbf{x}) - \rho(\mathbf{x}) = \mathrm{Bias}(\hat{\rho}(\mathbf{x})) + \mathcal{V}(\hat{\rho}(\mathbf{x}))\,, \tag{20a}$$

with

$$\mathrm{Bias}(\hat{\rho}(\mathbf{x})) = \rho(\mathbf{x}) - \mathbb{E}\left(\hat{\rho}(\mathbf{x})\right)\,, \qquad \mathcal{V}(\hat{\rho}(\mathbf{x})) = \hat{\rho}(\mathbf{x}) - \mathbb{E}\left(\hat{\rho}(\mathbf{x})\right)\,. \tag{20b}$$

The bias of the estimator denoted $\mathrm{Bias}(\hat{\rho})(\mathbf{x})$ measures how close to the continuous density the most probable value of the statistical estimator is. This part of the approximation error depends on the mesh discretization as well as the smoothness of the solution (see Tab 1). It is therefore referred to as "grid based" error. The second error component, namely $\mathcal{V}(\hat{\rho})$, is a centered random variable. It provides a measure of the particle sample dispersion, around the most probable value of the estimator. It is referred to as numerical noise or statistical error and estimated by means of the variance of $\mathcal{V}(\hat{\rho}(\mathbf{x}))$ defined as

$$\mathbb{V}(\mathcal{V}(\hat{\rho}) = \mathbb{E}\big(\mathcal{V}(\hat{\rho})^2\big) - \big(\mathbb{E}(\mathcal{V}(\hat{\rho}))\big)^2 \tag{20c}$$

The error estimates related to the regular PIC method, the Sparse-PIC method and the Offset Sparse-PIC methods are gathered in tab 1, we refer to [6] and the reference herein for their derivation. These estimates characterise the bias and the numerical noise of the statistical estimator of the either the density and the electic field, the sparse surrogates being considered for the the Sparse-PIC approximations.

	$\|\operatorname{Bias}(\hat{\rho}_{h_n})\|_\infty$ / $\|\operatorname{Bias}(\hat{\rho}^c_{h_n})\|_\infty$	$\mathbb{V}(\mathcal{V}(\hat{\rho}_{h_n}))^{\frac{1}{2}}$ / $\mathbb{V}(\mathcal{V}(\hat{\rho}^c_{h_n}))^{\frac{1}{2}}$
PIC	$h_n^2(\sum_{i=1}^d \partial_i^2\rho)$	$(Nh_n^d)^{-\frac{1}{2}}\|\rho\|_\infty$
S-P	$h_n^2\,\lvert\log h_n\rvert^{d-1}\left\|\partial_1^2\ldots\partial_d^2\rho\right\|_\infty$	$(Nh_n)^{-\frac{1}{2}}\lvert\log h_n\rvert^{d-1}\|\rho\|_\infty$
OS-P	$h_{n_2}^2\lvert\log h_{n_1}\rvert^{d-1}\|\partial_1^2\ldots\partial_d^2\rho\|_\infty$	$(Nh_{n_2})^{-\frac{1}{2}}\lvert\log h_{n_1}\rvert^{d-1}\|\rho\|_\infty$
	$\|\operatorname{Bias}(E_{h_n})\|_\infty$ / $\|\operatorname{Bias}(E^c_{h_n})\|_\infty$	$\mathbb{V}(\mathcal{V}(E_{h_n}))^{\frac{1}{2}}$ / $\mathbb{V}(\mathcal{V}(E^c_{h_n}))^{\frac{1}{2}}$
PIC	$h_n^2\sum_{i=1}^d(\|\nabla\partial_1^2\partial_i^2\rho\|_\infty + \left\|\partial_i^4 E\right\|_\infty)$	$(Nh_n^d)^{-\frac{1}{2}}\|\nabla\rho\|_\infty$
S-P	$h_n^2\,\lvert\log h_n\rvert^{d-1}\left\|\partial_1^4\ldots\partial_d^4 E\right\|_\infty$	$(Nh_n)^{-\frac{1}{2}}\lvert\log h_n\rvert^{d-1}\|\nabla\rho\|_\infty$
OS-P	$h_{n_2}^2\lvert\log h_{n_1}\rvert^{d-1}\|\partial_1^4\ldots\partial_d^4 E\|_\infty$	$(Nh_{n_2})^{-\frac{1}{2}}\lvert\log h_{n_1}\rvert^{d-1}\|\nabla\rho\|_\infty$

Table 1: Comparison of the dominant terms of the error estimates for the charge density $\hat{\rho}$ and electric field E issued from the PIC, Sparse-PIC (S-P) and Offset Sparse-PIC (OS-P) methods. This error estimates are related to second order space accurate methods and characterize the recombined sparse grid surrogates for sparse grid approximations, the parameters (n_1, n_2) of the offset method being defined by Eq. (19)

Regarding the grid based error of the different methods, it is roughler proportional to the square of the mesh size h_n^2 which is line with the space second order accuracy claimed for these methods. A more subtel analysis shows that, for Sparse-PIC methods, the dominant temr in the grid based error is multiplied by a factor $\log(h_n)^{d-1}$ which is an estimation of the total number of component grids populating the sparse grid hierarchy. This outlines the advantage of the offset Sparse-PIC methods. For this class of methods this term is indeed reduced to $\log(h_{n_1})^{d-1}$ where n_1 is defined by eq. (19) with $n_1 \leq n$. This improvement on the grid based error is consolidated by the improved resolution of the componnent grids related to $n_2 \geq n$. To conclude the analysis of the bias, it is important to note that this component of the error is dependent of higher order derivatives of the solution for Sparse-PIC methods compared to the regular PIC methods, which in the end is detrimental to the precision.

The picture is quite different for the statiscal noise carried by the approximations issued from these methods. First, the statistical noise of the regular PIC methods is not solely contingent on the total particle count N but rather on the average particle per cell, more specically on its square root $(Nh_n^d)^{1/2}$. This outlines that iproving the mesh resolution improves the grid based error but increases the numerical noise, in particular for problems with high dimensionality. Whereas increasing the particle count mitigates the statistical precision without compromising the grid accuracy. This asymmetry, coupled with the slow square root dependence, frequently results in a numerical noise dominating the total error. The improvements of Sparse-PIC methods regarding the control of the statistical noise is clearly outlined here, the term $(Nh_n^d)^{1/2}$ being substituted by $(Nh_n)^{-1/2}|\log(h_n)|^{d-1}$ which is weakly dependent of the dimensionality of the problem. The gains are all the more effective than the dimensionality of the problem is high. These estimates also highlights that the gains obtained of the grid based error of the offset method are detrimental to the statiscal noise.

These conclusions call for the exploration of opportunities for improving the grid error without reverting on the progress made in mitigating the numerical noise. This is the aim of the high-high-orderorder Sparse-PIC methods introduced in the next section.

3 High-order sparse-PIC methods

3.1 Definitions of high-order shape and basis functions

The sparse-PIC methods stand to benefit from grid error improvements, as this is where they currently fall short compared to the standard methods. Our aim here is to maintain the noise reduction enhancements while independently increasing grid error. The idea is that we reach 2^{nd} order grid-discretization dependence only by parity. By removing the lock of the second order moment i.e. nullify it, we could reach a 4^{th} order convergence. More precisely, to advance to higher orders, a theorem known as the moments condition informs us that we must nullify as much moments as the order we want to reach for our shape function. Delve into detailed developments by consulting

[4] equation (7.2.5). Consequently, we will construct functions designed to satisfy this requirement. For building high-order method, we will need high-order approximation function, in particular we might consider the W^p ones, for $p = 2, 4, 6$, details about computation could be found in [19].

$$W^2(x) = \begin{cases} 1 - |x| & \text{if } |x| \leq 1 \\ 0 & \text{otherwise.} \end{cases} \tag{21}$$

$$W^4(x) = \begin{cases} \frac{1}{2}|x|^3 - |x|^2 - \frac{1}{2}|x| + 1 & \text{if } |x| \leq 1 \\ -\frac{1}{6}|x|^3 + |x|^2 - \frac{11}{6}|x| + 1 & \text{if } 1 \leq |x| \leq 2 \\ 0 & \text{otherwise.} \end{cases} \tag{22}$$

$$W^6(x) = \begin{cases} \frac{1}{4}|x|^5 - \frac{1}{8}|x|^4 + \frac{3}{8}|x|^3 - \frac{5}{4}|x|^2 + \frac{1}{3}|x| - \frac{1}{12} & \text{if } |x| \leq 1 \\ \frac{1}{24}|x|^5 - \frac{1}{8}|x|^4 + \frac{25}{24}|x|^3 - \frac{5}{8}|x|^2 - \frac{13}{12}|x| + \frac{1}{24} & \text{if } 1 \leq |x| \leq 2 \\ -\frac{1}{720}|x|^5 + \frac{1}{16}|x|^4 - \frac{17}{48}|x|^3 + \frac{5}{16}|x|^2 - \frac{137}{60}|x| + \frac{1}{120} & \text{if } 2 \leq |x| \leq 3 \\ 0 & \text{otherwise.} \end{cases} \tag{23}$$

These functions verify the crucial following properties:

- Partition of unity:
$$\forall \mathbf{x} \in \Omega_x, \quad \sum_{j \in \mathbf{I}_{h_\mathbf{l}}} W^p((\mathbf{x} - \mathbf{j}h_\mathbf{l})h_\mathbf{l}^{-1}) = 1. \tag{24}$$

- Parity:
$$\forall \mathbf{x} \in \Omega_x, \;\; W^p(\mathbf{x}) = W^p(-\mathbf{x}). \tag{25}$$

- Unit mean:
$$\int_{\Omega_x} W^p(\mathbf{x}) d\mathbf{x} = 1. \tag{26}$$

Sometimes we have to compute derivatives of the basis function but these functions are only continuous. Beside the main problem of sparse grid are the heterogeneous case with high gradient so reaching higher smooth degree of smoothness could be an alternative. We can choose B-Spline but we don't want to loose the accuracy we won before, so we build a high-order high-regularity function. We choose a second degree of smoothness and a fourth order accuracy for the following V_2^4 function:

$$V_2^4(x) = \begin{cases} \frac{1}{6}|x|^5 - \frac{1}{3}|x|^4 + \frac{5}{4}|x|^3 - \frac{5}{4}|x|^2 + \frac{8}{10} & \text{if } |x| \leq 1 \\ \frac{1}{24}|x|^5 - \frac{3}{8}|x|^4 + \frac{25}{24}|x|^3 - \frac{5}{8}|x|^2 - \frac{5}{4}|x| + \frac{13}{10} & \text{if } 1 \leq |x| \leq 2 \\ -\frac{1}{120}|x|^5 + \frac{1}{8}|x|^4 - \frac{17}{24}|x|^3 + \frac{15}{8}|x|^2 - \frac{9}{4}|x| + \frac{9}{10} & \text{if } 2 \leq |x| \leq 3 \\ 0 & \text{otherwise.} \end{cases} \tag{27}$$

3.2 Error estimates : main results

In this section, we introduce the main results of this paper concerning the sparse-PIC methods with the high-order low-regularity shape and basis functions W^p, where $p = 2, 4, 6$ denote the order of these functions. We introduce the following functional spaces:

$$\mathcal{C}^\alpha(\Omega_x) := \left\{ u : \Omega_x \to \mathbb{R} \mid D^{\boldsymbol{\beta}} u \in \mathcal{C}(\Omega_x), \; \forall \|\boldsymbol{\beta}\|_1 \leq \alpha \right\}, \tag{28}$$

$$X^\alpha(\Omega_x) := \left\{ u : \Omega_x \to \mathbb{R} \mid D^{\boldsymbol{\beta}} u \in \mathcal{C}(\Omega_x), \; \forall \|\boldsymbol{\beta}\|_\infty \leq \alpha \right\}, \tag{29}$$

where $\mathcal{C}(\Omega)$ denotes the space of continuous functions on Ω_x.

Theorem 3.1 (Electric field) *The local errors between the sparse grid reconstructions and the solutions are recast into a grid-based error and a particle sampling error:*

$$\boldsymbol{E}_{h_n}^c - \boldsymbol{E} = Bias(\boldsymbol{E}_{h_n}^c) + \mathcal{V}(\boldsymbol{E}_{h_n}^c). \tag{30}$$

Assuming enough smoothness on the solution, i.e. $\boldsymbol{E} \in X^{p+2}(\Omega)$, $\rho \in X^{p+2}(\Omega) \cap \mathcal{C}^{p+3}(\Omega)$, *the*

following bounds for the grid-based and particle sampling errors hold true:

$$\left\|Bias(\boldsymbol{E}^c_{h_n})\right\|_\infty \leq K_{\boldsymbol{E}} h_n^p |\log h_n|^{d-1} + O\big(h_n^p |\log h_n|^{d-2}\big)\,, \tag{31}$$

$$\|\mathbb{V}(\mathcal{V}(\boldsymbol{E}^c_{h_n}))^{\frac{1}{2}}\|_\infty \leq D_{\boldsymbol{E}} (Nh_n)^{-\frac{1}{2}} |\log h_n|^{d-1} + O\left(\left(\frac{|\log h_n|^{d-1}}{Nh_n}\right)^{\frac{1}{2}}\right). \tag{32}$$

where $K_{\boldsymbol{E}}, D_{\boldsymbol{E}}$ are constants, provided in the appendix, depending on the dimension d and the derivatives of $\rho, \boldsymbol{E}$.

Theorem 3.2 (Charge density) *The local errors between the sparse grid reconstructions and the solutions are recast into a grid-based error and a particle sampling error:*

$$\hat{\rho}^c_{h_n} - \rho = Bias(\hat{\rho}^c_{h_n}) + \mathcal{V}(\hat{\rho}^c_{h_n}), \tag{33}$$

Assuming enough smoothness on the solution, i.e. $\rho \in X^p(\Omega)$, the following bounds for the grid-based and particle sampling errors hold true:

$$\|Bias(\hat{\rho}^c_{h_n})\|_\infty \leq K_\rho h_n^p |\log h_n|^{d-1} + O\big(h_n^p |\log h_n|^{d-2}\big)\,, \tag{34}$$

$$\left\|\mathbb{V}\left(\mathcal{V}(\hat{\rho}^c_{h_n})\right)^{\frac{1}{2}}\right\|_\infty \leq D_\rho (Nh_n)^{-\frac{1}{2}} |\log h_n|^{\frac{d-1}{2}} + O\Big(|\log h_n|^{d-1} N^{-\frac{1}{2}}\Big)\,, \tag{35}$$

where K_ρ, D_ρ are constants, provided in the appendix, depending on the dimension d and the derivatives of ρ.

By comparing the results obtained in this study with those presented in [6], it becomes evident that the statistical noise remains consistent for sparse-PIC methods employing functions of order 2, 4 or 6. This outcome is crucial, as it ensures that increasing the order enhances grid accuracy while leaving particle sampling error unaffected.

Corollary 3.3 (particle sampling error comparison) *Let $P_c \in \mathbb{N}$ being an integer representing the mean number of particles per cell, and considering a total number of particles N defined by the following equations for the sparse-PIC and standard PIC schemes:*

$$N_{std} = P_c h_n^{-d}, \quad N_{sparse} = P_c \left(\sum_{l \in \mathbb{L}} |c_l| h_{l_1} ... h_{l_d}\right)^{-1}. \tag{36}$$

Then the particle sampling error of the reconstructed charge density with sparse-PIC scheme is comparable to the one of the standard PIC methods:

$$\mathbb{V}\left(\mathcal{V}(\hat{\rho}_{h_n})\right)^{\frac{1}{2}} = \left(\frac{D_{std}\mathcal{Q}\rho}{P_c}\right)^{\frac{1}{2}}, \quad \mathbb{V}\left(\mathcal{V}(\hat{\rho}^c_{h_n})\right)^{\frac{1}{2}} \leq \left(\frac{D_{sg}\mathcal{Q}\rho}{P_c}\right)^{\frac{1}{2}}, \tag{37}$$

where D_{std} and D_{sg} are constants that depends only on the dimension.

3.2.1 Proofs of the main results

Theorem 3.1 extends the result of Proposition 3.8 in [6] to encompass high-order shape and basis functions denoted as W^p. The proof for the particle sampling error in Theorem 3.1 result aligns with that presented in [6], and we direct the reader to that work for a comprehensive understanding. To establish the grid-based error result, we introduce specific notations and Lemmas in the following.

Definition 3.4 *Let us introduce the notation $\{i_1, ..., i_m\} \in \mathbb{I} := \{\emptyset, \{1\}, \{2\}, \{3\}, \{1,2\}, \{2,3\}, \{1,3\}, \{1,2,3\}\}$, for $0 \leq m \leq d$ which stand for:*

$$\{i_1, ..., i_m\} := \begin{cases} \emptyset \quad \textit{if } m = 0, \\ \{1\} \textit{ or } \{2\} \textit{ or } \{3\} \quad \textit{if } m = 1, \\ \{1,2\} \textit{ or } \{2,3\} \textit{ or } \{1,3\} \quad \textit{if } m = 2, \\ \{1,2,3\} \quad \textit{if } m = 3. \end{cases} \tag{38}$$

The quantities (function ,domain, operator, etc.) associated with this notation correspond either to continuous ones ($m = 0$), semi-discrete ones ($m = 1$, $m = 2$) or discrete ones ($m = 3$). For example, the Laplacian is defined by:

$$\Delta_{h_l}^{(i_1,...,i_m)} u = \sum_{k\in\{i_1,...,i_m\}} \Delta_{h_{l_k}} u + \sum_{\substack{k\in\{1,...,d\}\\ k\notin\{i_1,...,i_m\}}} \partial_k^2 u, \tag{39}$$

for u a function defined on the hyperplane:

$$\Omega_{h_l}^{(i_1,...,i_m)} := \{\boldsymbol{x}\in\Omega \mid x_{i_k} \in \{j h_{l_{i_k}} \mid 0 \le j \le h_{l_{i_k}}^{-1}\}, 1 \le k \le m\},\ \ \Omega_{h_l}^{\emptyset} := \Omega. \tag{40}$$

$\Delta_{h_{l_k}} u$ is the discrete one dimensional p^{th} order Laplacian operator defined by finite differences.

Lemma 3.5 (Projection error) *Let $f(\cdot,\boldsymbol{v}) \in X^p(\Omega)$, then the grid-based error and the particle sampling errors verify the local errors:*

$$Bias(\hat{\rho}_{h_l})(\boldsymbol{x}) = \sum_{m=1}^{d} \sum_{\substack{\{i_1,...,i_m\}\\ \subset\{1,...,d\}}} b_{i_1,...,i_m}(\boldsymbol{x}; h_{l_{i_1}},...,h_{l_{i_m}}) h_{l_{i_1}}^p ... h_{l_{i_m}}^p \tag{41}$$

$$\mathbb{V}(\mathcal{V}(\hat{\rho}_{h_l})(\boldsymbol{x}))^{\frac{1}{2}} = \left(\frac{C_{part}^d \mathcal{Q}\rho(\boldsymbol{x})}{N h_{l_1}...h_{l_d}}\right)^{\frac{1}{2}} + O\left(N^{-\frac{1}{2}}\right), \tag{42}$$

where

$$b_{i_1,...,i_m}(\boldsymbol{x}; h_{l_{i_1}},...,h_{l_{i_m}}) = C_{bias}^m \partial_{i_1}^p ... \partial_{i_m}^p \rho(\boldsymbol{x}) + O\left(h_{l_{i_1}}^2,...,h_{l_{i_m}}^2\right), \tag{43}$$

$$C_{bias} = \begin{cases} \frac{1}{12} \text{ for } p=2, \\ \frac{5687}{5760} \text{ for } p=4, \end{cases},\ \ C_{part} = \begin{cases} \frac{2}{3} \text{ for } p=2, \\ \frac{733}{945} \text{ for } p=4, \end{cases} \tag{44}$$

Lemma 3.6 (Truncation error of semi-discrete laplacian and gradient) *Let $u \in \mathcal{C}^{p+2}(\Omega_{h_l}^{(i_1,...,i_m)})$, where $\{i_1,...,i_m\} \in \mathbb{I}$, $0 \le m \le d-1$, then:*

$$\left(\Delta_{h_l} - \Delta_{h_l}^{(i_1,...,i_m)}\right) u(\boldsymbol{x}) = \sum_{\substack{k\in\{1,...,d\}\\ k\notin\{i_1,...,i_m\}}} \tau_k(\boldsymbol{x}; h_{l_k}) h_{l_k}^p, \tag{45}$$

$$\left(\boldsymbol{\nabla}_{h_l} - \boldsymbol{\nabla}_{h_l}^{(i_1,...,i_m)}\right) u(\boldsymbol{x}) = \left(s_k(\boldsymbol{x}; h_{l_k}) h_{l_k}^p\right)_{\substack{k\in\{1,...,d\}\\ k\notin\{i_1,...,i_m\}}} \tag{46}$$

with

$$\|\tau_k(\cdot; h_{l_k})\|_\infty \le C_{lap} \|\partial_k^{p+2} u\|_\infty,\ \ \|s_k(\cdot; h_{l_k})\|_\infty \le C_{grad} \|\partial_k^{p+1} u\|_\infty \tag{47}$$

$$C_{lap} = \begin{cases} \frac{1}{12} \text{ for } p=2, \\ \frac{1}{90} \text{ for } p=4. \end{cases},\ \ C_{grad} = \begin{cases} \frac{1}{3} \text{ for } p=2, \\ \frac{2}{5} \text{ for } p=4. \end{cases} \tag{48}$$

Lemma 3.7 (Maximum principle) *Let $u \in C^2\left(\Omega_{h_l}^{(i_1,...,i_m)}\right)$, $w \in C^0\left(\Omega_{h_l}^{(i_1,...,i_m)}\right)$, where $\{i_1,...,i_m\} \in \mathbb{I}$ and $0 \le m \le 2$, verifying the semi-discrete problem:*

$$\left(\Delta_{h_l}\right)^{(i_1,...,i_m)} u = w, \quad u_{|\partial\Omega} = 0, \tag{49}$$

then the following majoration holds:

$$\|u\|_\infty \le C_{max} \|w\|_\infty, \quad i.e.\ \ \left\|\left(\Delta_{h_l}^{(i_1,...,i_m)}\right)^{-1}\right\|_\infty \le C_{max},\ \ C_{max} = \frac{1}{8}. \tag{50}$$

Lemma 3.8 (Semi-discrete interpolation error on V_{h_l}) *Let $u \in X^p\left(\Omega_{h_l}^{(i_1,\dots,i_m)}\right)$, where $\{i_1,\dots,i_m\} \in \mathbb{I}$ and $0 \leq m \leq d-1$, then the local error at $\boldsymbol{x} \in \Omega_{h_l}^{(i_1,\dots,i_m)}$ of the interpolation onto V_{h_l} is:*

$$\mathcal{I}_{V_{h_l}} u(\boldsymbol{x}) - u(\boldsymbol{x}) = \tag{51}$$
$$\sum_{k=1}^{d-m} \sum_{\substack{\{r_1,\dots,r_k\}\subset\{1,\dots,d\} \\ s.t.\ \{r_1,\dots,r_k\}\cap\{i_1,\dots,i_m\}=\emptyset}} d_{i_1,\dots,i_m;r_1,\dots,r_k}(\boldsymbol{x}; h_{l_{i_1}},\dots,h_{l_{i_m}}; h_{l_{r_1}},\dots,h_{l_{r_k}}) h_{l_{r_1}}^p \dots h_{l_{r_k}}^p,$$

where

$$\|d_{i_1,\dots,i_m;r_1,\dots,r_k}(\cdot; h_{l_{i_1}},\dots,h_{l_{i_m}}; h_{l_{r_1}},\dots,h_{l_{r_k}})\|_\infty \leq C_{int}^k \|\partial_{r_1}^p \dots \partial_{r_k}^p u\|_\infty, \tag{52}$$

$$C_{int} = \begin{cases} \dfrac{4}{27} \text{ for } p=2, \\ 0.237 \text{ for } p=4. \end{cases} \tag{53}$$

Lemma 3.9 (Combination) *Let u be a function and $u_{h_l} \in V_{h_l}$ be an approximation of u such that the following pointwise error expansion holds:*

$$u_{h_l}(\boldsymbol{x}) - u(\boldsymbol{x}) = \sum_{m=1}^{d} \sum_{\substack{\{i_1,\dots,i_m\} \\ \subset\{1,\dots,d\}}} c_{i_1,\dots,i_m}(\cdot; h_{l_{i_1}},\dots,h_{l_{i_m}}) h_{l_{i_1}}^p \dots h_{l_{i_m}}^p, \tag{54}$$

where the $c_{i_1,\dots,i_m}(\cdot; h_{l_{i_1}},\dots,h_{l_{i_m}})$ are bounded functions by a constant κ, then the combination verifies:

$$\|u_{h_n}^c - u\|_\infty \leq C_{comb} \kappa h_n^p |\log h_n|^{d-1} + O\left(h_n^p |\log h_n|^{d-2}\right), \tag{55}$$

$$C_{comb} = \begin{cases} \dfrac{5}{4} \text{ for } d=2, \\ \dfrac{65}{32} \text{ for } d=3. \end{cases} \tag{56}$$

Proof of Lemmas 3.5, 3.6, 3.7, 3.8, 3.9. The proofs of the Lemmas are detailed in the appendix.
Proof of Theorem 3.1. First the local error is recast into:

$$\mathcal{I}_{V_{h_1}} \mathbf{E}_{h_1} - \mathbf{E} = \mathcal{I}_{V_{h_1}} (\mathbf{E}_{h_1} - \mathbf{E}) + \mathcal{I}_{V_{h_1}} \mathbf{E} - \mathbf{E}. \tag{57}$$

In the following the dependance on the grid discretization of the coefficients of the form $b_{i_1,\dots,i_m}(\cdot; h_{l_{i_1}},\dots,h_{l_{i_m}})$ is omitted for simplicity of notation. Applying Lemma 3.6 in the continuous case ($m=0$) and introducing the estimator of the density from Lemma 3.5, one gets:

$$\Delta_{h_1}\Phi + \hat{\rho}_{h_1} = \sum_{i=1}^{3} (b_i + \tau_i) h_{l_i}^p + \sum_{\substack{i,j=1 \\ i\neq j}}^{3} b_{i,j} h_{l_i}^p h_{l_j}^p + b_{1,2,3} h_{l_1}^p h_{l_2}^p h_{l_3}^p + \mathcal{V}(\hat{\rho}_{h_1}). \tag{58}$$

Let us introduce the semi-discrete problems for $w_i \in \Omega_{h_1}^{(i)}$, $w_{i,j} \in \Omega_{h_1}^{(i,j)}$, with $i,j \in \{1,2,3\}$, $i \neq j$:

$$-\left(\Delta_{h_1}\right)^{(i)} w_i = b_i + \tau_i, \quad -\left(\Delta_{h_1}\right)^{(i,j)} w_{i,j} = b_{i,j}. \tag{59}$$

It follows:

$$\begin{aligned}\Delta_{h_1}\Big(\Phi+\sum_{i=1}^{3} w_i h_{l_i}^p+\sum_{\substack{i,j=1\\ i\neq j}}^{3} w_{i,j} h_{l_i}^p h_{l_j}^p\Big)+\hat{\rho}_{h_1} &= \sum_{i=1}^{3}\Big(\Delta_{h_1}-\Delta_{h_1}^{(i)}\Big) w_i h_{l_i}^p \\ &+\sum_{\substack{i,j=1\\ i\neq j}}^{3}\Big(\Delta_{h_1}-\Delta_{h_1}^{(i,j)}\Big) w_{i,j} h_{l_i}^p h_{l_j}^p + b_{1,2,3} h_{l_1}^p h_{l_2}^p h_{l_3}^p + \mathcal{V}(\hat{\rho}_{h_1}) \\ &= \sum_{\substack{i,j=1\\ i\neq j}}^{3} \tilde{w}_{i,j} h_{l_i}^p h_{l_j}^p + (\tilde{w}_{1,2,3}+b_{1,2,3}) h_{l_1}^p h_{l_2}^p h_{l_3}^p + \mathcal{V}(\hat{\rho}_{h_1}),\end{aligned}$$

where Lemma 3.6 has been applied twice and thanks to Lemma 3.7:

$$\|\tilde{w}_{i,j}\|_\infty \leq C_{max}\left(C_{bias}C_{lap}\|\partial_i^p\partial_j^{p+2}\rho\|_\infty + C_{lap}^2\|\partial_i^{p+2}\partial_j^{p+2}\Phi\|_\infty\right), \tag{60}$$

$$\|\tilde{w}_{1,2,3}\|_\infty \leq C_{max}C_{bias}^2C_{lap}\sum_{i,j,k}\|\partial_i^{p+2}\partial_j^p\partial_k^p\rho\|_\infty. \tag{61}$$

We introduce the following semi-discrete problems for $\gamma_{i,j}\in\Omega_{h_1}^{(i,j)}$, with $i,j\in\{1,2,3\}$, $i\neq j$:

$$-\left(\Delta_{h_1}\right)^{(i,j)}\gamma_{i,j} = \tilde{w}_{i,j}, \tag{62}$$

so that it holds:

$$\begin{aligned}\Delta_{h_1}\Big(\Phi+\sum_{i=1}^{3} w_i h_{l_i}^p+\sum_{\substack{i,j=1\\ i\neq j}}^{3}\left(w_{i,j}+\gamma_{i,j}\right) h_{l_i}^p h_{l_j}^p\Big)+\hat{\rho}_{h_1} &= \sum_{\substack{i,j=1\\ i\neq j}}^{3}\Big(\Delta_{h_1}-\Delta_{h_1}^{(i,j)}\Big)\gamma_{i,j} h_{l_i}^p h_{l_j}^p \\ &+(\tilde{w}_{1,2,3}+b_{1,2,3}) h_{l_1}^p h_{l_2}^p h_{l_3}^p + \mathcal{V}(\hat{\rho}_{h_1}) \\ &= w_{1,2,3} h_{l_1}^p h_{l_2}^p h_{l_3}^p + \mathcal{V}(\hat{\rho}_{h_1}),\end{aligned}$$

where Lemma 3.6 has been applied again and:

$$\begin{aligned}\|w_{1,2,3}\|_\infty \leq C_{bias}^3\|\partial_1^p\partial_2^p\partial_3^p\rho\|_\infty + \|\tilde{w}_{1,2,3}\|_\infty + 6C_{max}^2C_{lap}^3\|\partial_1^{p+2}\partial_2^{p+2}\partial_3^{p+2}\Phi\|_\infty \\ + C_{max}^2C_{bias}C_{lap}^2\sum_{i,j,k}\|\partial_i^p\partial_j^{p+2}\partial_k^{p+2}\rho\|_\infty.\end{aligned}$$

Applying the operators $(\Delta_{h_1})^{-1}$, $\boldsymbol{\nabla}_{h_1}$, $\boldsymbol{\nabla}_{h_1}^{(i)}$, $\boldsymbol{\nabla}_{h_1}^{(i,j)}$ which commute, and owing to Lemma 3.6 for the gradient, one gets:

$$\boldsymbol{\nabla}_{h_1}\Phi - \boldsymbol{\nabla}_{h_1}\Phi_{h_1} = \sum_{i=1}^{3}\mathbf{z}_i h_{l_i}^p + \sum_{\substack{i,j=1\\ i\neq j}}^{3}\mathbf{z}_{i,j} h_{l_i}^p h_{l_j}^p + \mathbf{z}_{1,2,3} h_{l_1}^p h_{l_2}^p h_{l_3}^p + \hat{\mathcal{Z}}_{h_1}, \tag{63}$$

with $\mathbf{z}_i$,$\mathbf{z}_{i,j}$, $\mathbf{z}_{1,2,3}$ and $\hat{\mathcal{Z}}_{h_1}$ depending (in a way that shall be explicited later) on the derivatives of ρ and Φ. Lemma 3.6 for the gradient gives us:

$$\boldsymbol{\nabla}\Phi - \boldsymbol{\nabla}_{h_1}\Phi = \left(s_i h_{l_i}^p\right)_{i=1,2,3}, \quad \|s_i\|_\infty \leq C_{grad}\|\partial_i^{p+1}\Phi\|_\infty, \quad i=1,2,3, \tag{64}$$

so that adding equations (63) and (64):

$$\mathbf{E}_{h_1} - \mathbf{E} = \sum_{i=1}^{3}\tilde{\mathbf{z}}_i h_{l_i}^p + \sum_{\substack{i,j=1\\ i\neq j}}^{3}\mathbf{z}_{i,j} h_{l_i}^p h_{l_j}^p + \mathbf{z}_{1,2,3} h_{l_1}^p h_{l_2}^p h_{l_3}^p + \hat{\mathcal{Z}}_{h_1}, \tag{65}$$

with:

$$\|\tilde{\mathbf{z}}_i\|_\infty \leq C_{max}\left(C_{bias}\|\partial_i^p \boldsymbol{\nabla}\rho\|_\infty + C_{lap}\|\partial_i^{p+2}\mathbf{E}\|_\infty\right) + \max(\|s_1\|_\infty, \|s_2\|_\infty, \|s_3\|_\infty),$$

$$\|\mathbf{z}_{i,j}\|_\infty \leq C_{max}\Big(C_{bias}^2\|\partial_i^p\partial_j^p\boldsymbol{\nabla}\rho\|_\infty + \|\boldsymbol{\nabla}\tilde{w}_{i,j}\|_\infty + C_{grad}\Big(C_{bias}\|\partial_i^p\partial_j^{p+1}\boldsymbol{\nabla}\rho\|_\infty + C_{lap}(\|\partial_i^{p+2}\partial_j^{p+1}\mathbf{E}\|_\infty\Big)\Big),$$

$$\|\mathbf{z}_{1,2,3}\|_\infty \leq C_{max}\Big(\|\boldsymbol{\nabla}w_{1,2,3}\|_\infty + C_{grad}\Big(C_{bias}^2\sum_{i,j,k}\|\partial_i^p\partial_j^p\partial_k^{p+1}\boldsymbol{\nabla}\rho\|_\infty$$

$$+ C_{max}\big(C_{bias}C_{lap}\sum_{i,j,k}\|\partial_i^p\partial_j^{p+1}\partial_k^{p+2}\mathbf{E}\|_\infty + C_{lap}^2\sum_{i,j,k}\|\partial_i^{p+2}\partial_j^{p+2}\partial_k^{p+1}\mathbf{E}\|_\infty\big)\Big)\Big)$$

$$\|\hat{\mathcal{Z}}_{h_1}\|_\infty \leq C_{max}\|\boldsymbol{\nabla}\mathcal{V}(\hat{\rho}_{h_1})\|_\infty$$

Applying Lemma 3.8:

$$\mathcal{I}_{V_{h_1}}\mathbf{E} - \mathbf{E} = \sum_{i=1}^{3}\mathbf{d}_i h_{l_i}^p + \sum_{\substack{i,j=1\\ i\neq j}}^{3}\mathbf{d}_{i,j}h_{l_i}^p h_{l_j}^p + \mathbf{d}_{1,2,3}h_{l_1}^p h_{l_2}^p h_{l_3}^p, \tag{66}$$

$$\mathcal{I}_{V_{h_1}}(\mathbf{E}_{h_1} - \mathbf{E}) = \mathbf{E}_{h_1} - \mathbf{E} + \mathbf{f}_{1,2,3}h_{l_1}^p h_{l_3}^p h_{l_3}^p \tag{67}$$

with:

$$\|\mathbf{d}_i\|_\infty \leq C_{int}\|\partial_i^p\mathbf{E}\|_\infty,\ \ \|\mathbf{d}_{i,j}\|_\infty \leq C_{int}^2\|\partial_i^p\partial_j^p\mathbf{E}\|_\infty,\ \ \|\mathbf{d}_{1,2,3}\|_\infty \leq C_{int}^3\|\partial_1^p\partial_2^p\partial_3^p\mathbf{E}\|_\infty,$$

$$\|\mathbf{f}_{1,2,3}\|_\infty \leq C_{int}^2\sum_{i,j,k}\|\partial_i^p\partial_j^p\tilde{\mathbf{z}}_k\|_\infty + C_{int}\sum_{i,j,k}\|\partial_i^p\mathbf{z}_{j,k}\|_\infty.$$

Eventually, summing equations (66) and (67), one gets:

$$\mathcal{I}_{V_{h_1}}\mathbf{E}_{h_1} - \mathbf{E} = \sum_{i=1}^{3}\mathbf{e}_i h_{l_i}^p + \sum_{\substack{i,j=1\\ i\neq j}}^{3}\mathbf{e}_{i,j}h_{l_i}^p h_{l_j}^p + \mathbf{e}_{1,2,3}h_{l_1}^p h_{l_2}^p h_{l_3}^p + \hat{\mathcal{Z}}_{h_1}, \tag{68}$$

with:

$$\|\mathbf{e}_i\|_\infty \leq \|\mathbf{d}_i\|_\infty + \|\tilde{\mathbf{z}}_i\|_\infty,\ \ \|\mathbf{e}_{i,j}\|_\infty \leq \|\mathbf{d}_{i,j}\|_\infty + \|\mathbf{z}_{i,j}\|_\infty, \tag{69}$$

$$\|\mathbf{e}_{1,2,3}\|_\infty \leq \|\mathbf{d}_{1,2,3}\|_\infty + \|\mathbf{z}_{1,2,3}\|_\infty + \|\mathbf{f}_{1,2,3}\|_\infty, \tag{70}$$

and eventually using the Lemma 3.9 we obtain the result for the grid-based error. □

The detailed proof of the Theorem 3.2 can be found in the appendix.

4 Numerical investigations

4.1 Setup and Notations

Let *Pcell* (or P_c) denote the mean number of particle per cell, then the total number of particle pet cell is defined by equation (36). n denotes the size of the Cartesian h_n grid we consider, for Sparse method, this is where the quantity are recombined. In this section, we will refer for PIC method as "Standard-PIC" or "st". Specifying the use of W^{m} as base function gives us Standard-PIC(m) or "stWm". All Sparse-PIC methods using W^{m} will be noted "Sparse-PIC(m)" or "sgWm" (for sparse-grid). We will add an extra "o"$\mathbf{k}$ with $\mathbf{k}$ the degree of offset we use. For example: Sparse-PIC(2)o2 or sgW2o2 is the Sparse-PIC method which use W^2 as base function with 2 levels of offsets. For all simulation, we choose periodic limits that adapt well to the different length of support for the basic functions we will use. Our domain is the square $[0, L]^2$; L will be express referring to the Debye length $\lambda_D = \sqrt{\frac{\epsilon_0 T_e k_B}{n_e q_e^2}}$. where k_B is the Boltzman constant. T_e, n_e, q_e are respectively the electron Temperature, the electron density and the electron charge.

4.2 Verifaction of 4^{th} order accuracy

Our main goal is to create a 4^{th} order sparse-PIC algorithm. For this purpose, the first simulation we conduct aim to reproduce numerically the 4^{th} order convergence described before. So we perform 1D unitary test on each step of our algorithm and compare them to the 2^{nd} order accurate Sparse-PIC method. In particular we want to focus on the step involving the shape function W^4 i.e. projection and interpolation, because they are results not as well establish as Finite-Difference. For this section we use as many particles as we could in order to remove or reduce at best the statistic noise: we throw around 10^{10} particles in the following process. We will see further that there are good reason to think that for low discretization grid, that's more than enough, but the same argument leads us to believe that for the biggest mesh, more is needed.

Figure 1 is the result after testing the projection phase. For a range of grid, we plot the L2-norm of the difference on the grid point between projection on the grid of 10^{10} particles drawn according to a distribution f and the accurate initial distribution f. The f distribution we choose is $f(x) = 1 + .2cos(2\pi x)$ which is always positive and periodic in [0;1]; to avoid boundary effect on our error we use periodic bound. This could be see as a 1D Landau damping simulation and the particles are homogeneously spread which reduce the noise. This is helpful because we can equate the total error to the grid error. As we reach the 4^{th} asymptotic convergence, we ascertain that there are a sufficient number of particles to render statistical noise negligible. This holds true for the second-order curve as well, as it carries a larger grid error and is, therefore, less affected by statistical noise; this curve does not perform better than the asymptotic curve. Hence, it is reasonable to believe that the asymptotic curve is also numerical, and that we have achieved it.

For the last point, we improve the statistic by considering 10 clusters of 10^{10} particles and gathering all of them together to reduce the prevailing random error.

Figure 2 is the same process apply to the interpolation phase. We initiate our particles on random points of our domain, then see the difference between the exact density and the computed one by interpolation of the grid points. Because we have exact value on grid point, we don't have annoying noise to take account of. So there is no problem to see a 4^{th} convergence even a 6^{th} order convergence for large value of n i.e. for very tiny grid. As a result, see that the range of considered size of grid or discretion is wider than before. And for each size the numerical result match the theoretical maximum convergence.

4.3 Landau Damping

Landau Damping, a highly studied phenomenon, serves as a classic model for cases involving continuous and homogeneous particle distributions. Sparse-PIC methods have already demonstrated their effectiveness in addressing Landau Damping. One could view this test as an enhanced sanity check, but with a more practical perspective.

The initial data in Landau Damping is a perturbation in a Maxwellian equilibrium state of the distribution thus we consider the following distribution:

$$f_e(\mathbf{x}, \mathbf{v}) = \frac{1}{2\pi} \prod_{i=1}^{d} \left(1 + \alpha_i \cos\left(\frac{\beta_i 2\pi x}{L}\right)\right) e^{\frac{-||v||_2^2}{2}}$$

with the dimension $d = 2$; the amplitude $\alpha = (.20, .20)$ and period $\beta = (10, 10)$. Because of the high perturbation, we will call this "Strong Landau Damping". One can see that the considered period gives rise to 10 spike in each direction. The domain length L is $L = 160\lambda_D$ and will be approximated by a 128 by 128 mesh ; we count 128^2 cell in the Standard PIC method and 2560 in the Sparse one. Each cell will carry on average 2000 particles. Finally we choose a time-step $\Delta t = .05$ and an end time $t = 10$ i.e. 200 time loops.

In Figure 3 we have represented the error in the electric field in a base-10 logarithmic scale for Sparse/Standard-PIC methods with W^2/W^4 shape function. We observe the classical damping characteristic of this phenomenon. However, due to its strength, we do not discern linear effects. Furthermore, two key elements are noticeable. First, there is a decrease in peak amplitude between the Standard and the Sparse PIC methods, which is indicative of the scattering effect, leading to a reduction in the noise typically expected from Sparse methods [**?**]. Second, there is a phase shift between the second and fourth-order methods. We attribute this to a better approximation when approaching zero, which slows down the 2^{nd}-order methods but not the 4^{th}.

In Figures 4a, 4b, 4c, 4d, we chose to focus on a specific moment to observe the various density simulations. This moment correspond to few time-step before the second peak in Figure 3. We

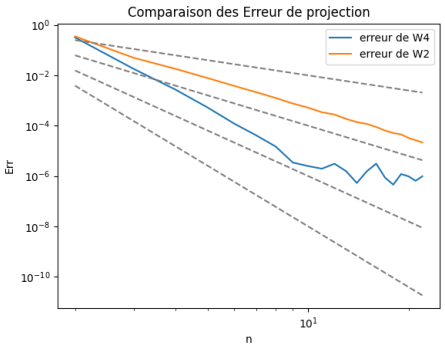

Figure 1: Validation of the 4^{th} order Projection: L2-error of the Projection of cosine distribution approximated with total 10^{11} particles on an increasing $2n$-points grid.

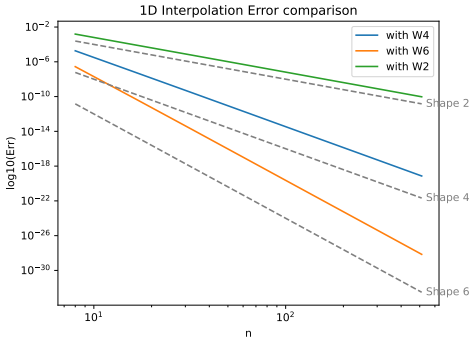

Figure 2: Validation of high order Interpolation: L2-Error comparison for sinusoidal function.

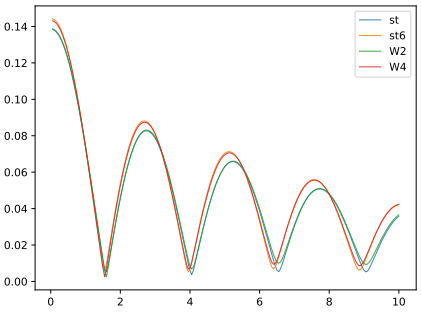

Figure 3: Landau Damping: Decimal logarithm of electrical energy for strong perturbation and various PIC methods

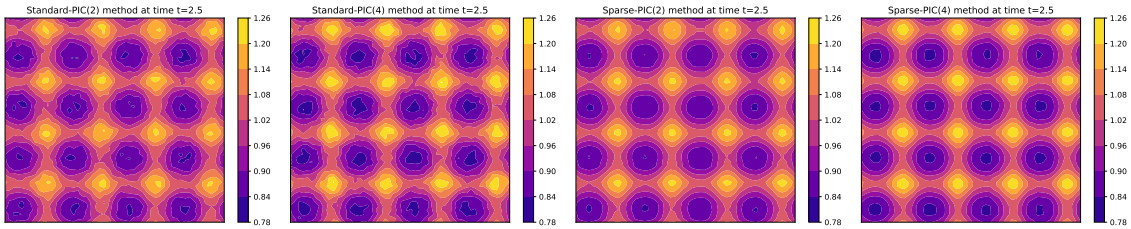

(a) Standard-PIC(2) (b) Standard-PIC(4) (c) Sparse-PIC(2) (d) Sparse-PIC(4)

Figure 4: Strong Landau Damping: Detail of contour curve for the density computed with various methods

compare Standard PIC method to Sparse-PIC method, using W^2 then W^4 shape functions for both methods. We retrieve the point we saw before but with a different angle. In Figures 4a and 4c, the achieved maxima are lower than those in Figures 4c and 4d, coinciding with the phase shift we saw earlier. Finally, a marked reduction in noise can be observed between Figures 4a and 4b, compared to Figures 4c and 4d, which exhibit a much smoother profile. This highlights the effectiveness of all the Sparse methods for this type of simulation. Using high order shape function maintain these good proprieties.

4.4 Diocotron instability

The Diocotron Instability is a challenging benchmark for Sparse methods, and we specifically selected it for this reason, aiming to outline the improvements brought about by the W^4 shape functions. We will also consider the embedding of high order methods with offset-Sparse PIC-method.

To represent this effect, we consider the following initial fluid particle distribution,

$$f_e(\mathbf{x},\mathbf{v}) = \frac{\gamma e^{-\frac{\left(\left\|\mathbf{x}-\frac{L}{2}\right\|_2-\frac{L}{4}\right)^2}{2(0.03L)^2}} e^{\frac{-\|\mathbf{v}\|_2^2}{2}}}{0.03L(2\pi)^2}$$

where $\|x\|_2^2 = \sum_{i=1}^d x_i^2$.γ is chosen to match the unit mean propriety of the distribution f_e. This time, an external magnetic field is added to the model, and is considered linear along the Z-axis, for our 2-dimension model, that mean $B = 15$ is constant on the X-Y plan, furthermore it is strong enough to dominate the electron dynamic.

Our domain length is $L = \frac{2\pi}{0.3}\lambda_D$. This domain will be approximated by a 256×256 mesh ; we count $256^2 = 65\ 536$ cells in the Standard PIC method and 5 888 cells i.e. 11 times less for the Sparse one. Each cell will carry on average 200 particles unlike the Landau Damping, this data should be regarded as a statistic and not as an observed mean behavior because most of the cell are empty. Finally we choose a time-step $\Delta t = .075$ and an end time $t = 75$ i.e. 1000 time steps.

Figure 5a serves as the reference solution against which numerical approximation will be compared. It exhibits numerous useful features warranting closer examination: density vertices with internal motion, filaments between them, and central symmetry.
The subsequent figures are all derived from the same simulation moment, parameterized under identical conditions. We will vary the shape functions and offset levels. Figure 5b corresponds to the Sparse-PIC(2) method, which represents the poorest performance and deviates significantly from the reference. Evident are the distinctive artifacts of the Sparse formalism, which reconstructs the solution along grid lines. The rotation differs as a consequence of the reconstruction, impeding proper simulation alignment. Filaments are poorly represented and symmetry is broken. Figure 5c, employing the Sparse-PIC(4) method, ameliorates the reconstruction issues along grid lines, aligning the formation better with the reference, although significant discrepancies persist, including interrupted filaments and coarse vertices.
Figure 5d combines $W6$ shape function and 2 levels of offset, demonstrating substantial improvement. While it doesn't match the reference perfectly, positive comparisons include enhanced representation of details like filaments and internal density vertices motion. Figure 5e, utilizing the V_2^4 shape

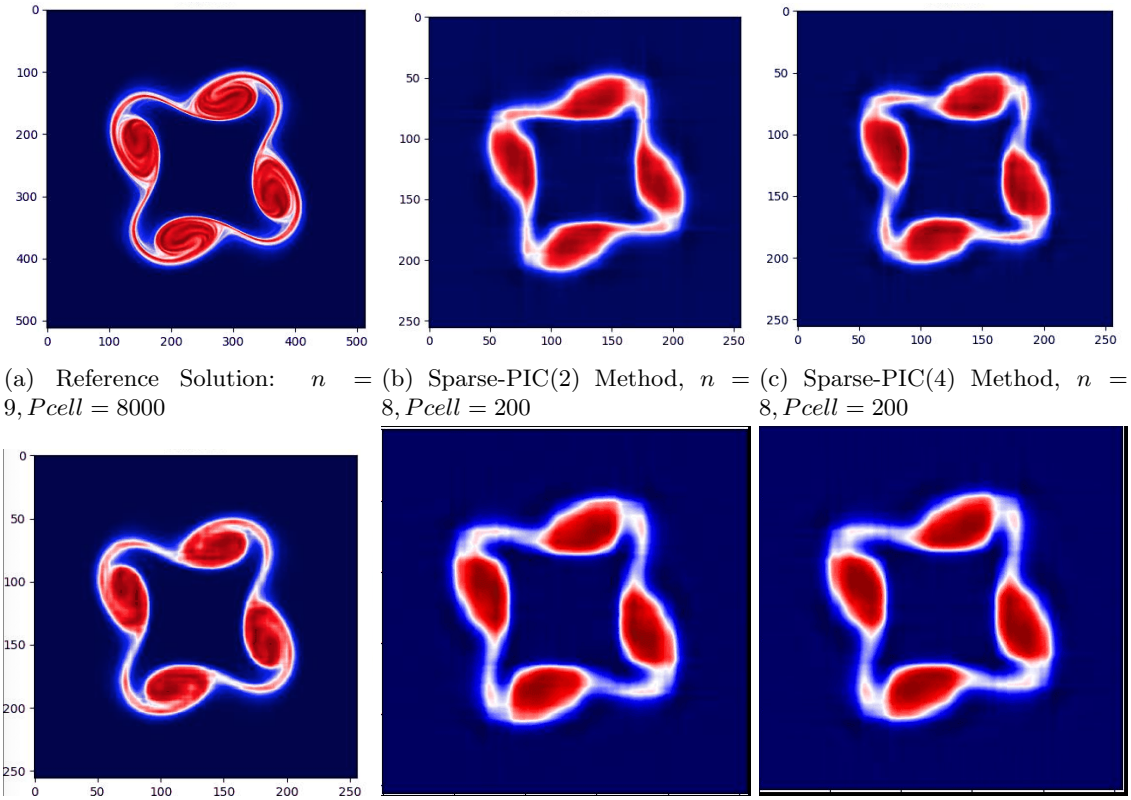

(a) Reference Solution: $n = 9, Pcell = 8000$

(b) Sparse-PIC(2) Method, $n = 8, Pcell = 200$

(c) Sparse-PIC(4) Method, $n = 8, Pcell = 200$

(d) Sparse-PIC(6)o2 Method, $n = 8, Pcell = 200$

(e) Sparse-PIC V_2^4 Method, $n = 8, Pcell = 200$

(f) Sparse-PIC V_4^4 Method, $n = 8, Pcell = 200$

Figure 5: Comparison of 6 methods in Diochotron Instability at time $t = 15$

function, yields relatively poor results, offering inadequate approximations despite substantial computational efforts. Figure 5f employs the V_4^4 shape function, and it is evident that this choice of a smoother function induces significant diffusion, adversely affecting method precision, especially in this particular case. It could even be argued that it performs less favorably than V_2^4.

In Figure 6, we compare a range of Sparse-PIC methods with different order and different levels of offset. We use a reference model which is a Standard-PIC method computed on a larger grid with more particles per cell than the considered methods, then we compute the normalized L1 error of the difference. We can see that Sparse-PIC(2) is worse that any other method, that's because the approximation is so bad that it reduce speed of rotation, conducing to an increasing difference whit the reference model. All the other methods get more accurate rotating speed, but with time most of them fail to capture the very thin detail of the Diochotron Instability conducing to an increasing error. If we improve accuracy order or offset level, we reduce the error. An interesting thing to see is that when we increase the order of a method, we "win" one level of offset. Multiple example can be found in 6: Sparse-PIC(4) method is doing better than Sparse-PIC(2)o1 and Sparse-PIC(4)o1 is really close to Sparse-PIC(2)o2.

In Figure 7, we focus on increasing the offset for Sparse-PIC(6) starting without any. We can see that high order method are still being improved by boosting offset technique. We can deduce 2 things: First, there is still room for more improvement. Second, the offset technique works better with higher order accurate method.

5 Conclusions

In this article, we introduce high-order shape and basis functions to enhance sparse-PIC methods. A comprehensive numerical analysis of the sparse quantities inherent in high-order schemes has been presented. This analysis has led to two significant outcomes. Firstly, by elevating the order

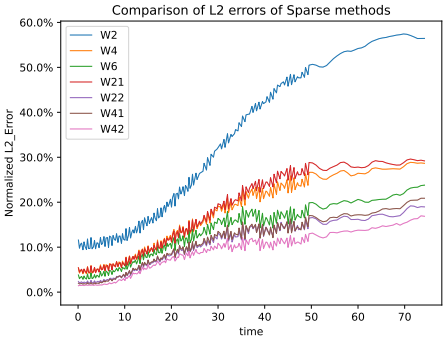

Figure 6: Normalized Error of various method for the Diochotron Instability, $n = 8, Pcell = 200$

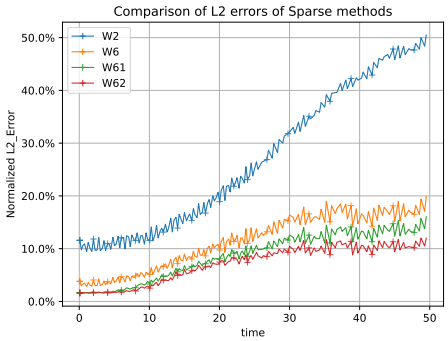

Figure 7: Improving offset on an high order method for the Diochotron Instability, $n = 8, Pcell = 200$

of accuracy of the schemes, we substantially alleviate the grid-based component of the error. This component is known to experience deterioration in complex configurations, thereby being identified as a primary drawback of sparse-PIC methods. Secondly, the particle sampling error of the high-order schemes remains equivalent to that of second-order schemes, ensuring that the introduction of higher-order functions does not compromise noise damping. Consequently, as demonstrated through numerical evidence, the high-order methods achieve improvements at a low cost, as the number of particles does not need to be increased, contrary to the offset method. Additionally, the benefits of high-order functions can be seamlessly integrated with offset methods to achieve more significant gains.

Acknowledgements

This work has been supported by a public grant from the "Laboratoire d'Excellence Centre International de Mathématiques et d'Informatique" (Labex CIMI) overseen by the French National Agency (ANR) as part of the "Investissement d'Avenir" program (reference ANR-11-LABX-0040) in the frame of the PROMETEUS project (PRospect of nOvel nuMerical modEls for elecTric propulsion and low tEmperatUre plaSmas).
Support from the "Fédération de Fusion pour la Recherche par Confinement Magnétique" (FrFCM) in the frame of the projects "BRIDIPIC: BRIDgIng Particle-In-Cell methods and low frequency numerical models of plasmas" and SPARCLE SParse grid Acceleration for the paRticle-in-CelL mEthod" is also acknowledged.
The authors acknowledge fruitful discussions with Laurent Garrigues and Gwenael Fubiani.

References

[1] C. Birdsall and A. Langdon. *Plasma Physics via Computer Simulation*. CRC Press, 0 edition, Oct. 2018.

[2] H.-J. Bungartz and S. Dirnstorfer. Higher Order Quadrature on Sparse Grids. In M. Bubak, G. D. van Albada, P. M. A. Sloot, and J. Dongarra, editors, *Computational Science - ICCS 2004*, Lecture Notes in Computer Science, pages 394–401, Berlin, Heidelberg, 2004. Springer.

[3] H.-J. Bungartz and M. Griebel. Sparse grids. *Acta Numerica*, 13:147–269, May 2004.

[4] G.-H. Cottet and P. D. Koumoutsakos. *Vortex Methods: Theory and Practice*. Typeface in Times Roman 10/13 pt. System LaTeX 2e. Cambridge University Press, Cambridge, 2000. This book is in copyright. Subject to statutory exception and to the provisions of relevant collective licensing agreements, no reproduction of any part may take place without the written permission of Cambridge University Press. First published 2000.

[5] J. M. Dawson. Particle simulation of plasmas. *Rev. Mod. Phys.*, 55(2):403–447, Apr. 1983. Publisher: American Physical Society.

[6] F. Deluzet, G. Fubiani, L. Garrigues, C. Guillet, and J. Narski. Sparse grid reconstructions for Particle-In-Cell methods. *ESAIM: M2AN*, 56(5):1809–1841, Sept. 2022.

[7] F. Deluzet, G. Fubiani, L. Garrigues, C. Guillet, and J. Narski. Efficient parallelization for 3d-3v sparse grid particle-in-cell: Shared memory architectures. *Journal of Computational Physics*, 480:112022, 2023.

[8] F. Deluzet, G. Fubiani, L. Garrigues, C. Guillet, and J. Narski. Efficient parallelization for 3d-3v sparse grid particle-in-cell: Single gpu architectures. *Computer Physics Communications*, 289:108755, 2023.

[9] R. E. Denton and M. Kotschenreuther. {delta}f Algorithm. Technical Report DOE/ET/53088-629; IFSR-629, Texas Univ., Austin, TX (United States). Inst. for Fusion Studies, Nov. 1993.

[10] J. Garcke. Sparse Grids in a Nutshell. In J. Garcke and M. Griebel, editors, *Sparse Grids and Applications*, volume 88, pages 57–80. Springer Berlin Heidelberg, Berlin, Heidelberg, 2012. Series Title: Lecture Notes in Computational Science and Engineering.

[11] L. Garrigues, M. Chung-To-Sang, G. Fubiani, C. Guillet, F. Deluzet, and J. Narski. Acceleration of Partcile-In-Cell Simulations using Sparse Grid Algorithmes. I Application to Dual Frequency Capacitive Discharges. In preparation.

[12] L. Garrigues, B. Tezenas du Montcel, G. Fubiani, F. Bertomeu, F. Deluzet, and J. Narski. Application of sparse grid combination techniques to low temperature plasmas particle-in-cell simulations. I. Capacitively coupled radio frequency discharges. *Journal of Applied Physics*, 129(15):153303, Apr. 2021. Publisher: American Institute of Physics.

[13] L. Garrigues, B. Tezenas du Montcel, G. Fubiani, and B. C. G. Reman. Application of sparse grid combination techniques to low temperature plasmas Particle-In-Cell simulations. II. Electron drift instability in a Hall thruster. *Journal of Applied Physics*, 129(15):153304, Apr. 2021. Publisher: American Institute of Physics.

[14] S. Gassama, E. Sonnendrücker, K. Schneider, M. Farge, and M. Domingues. Wavelet denoising for postprocessing of a 2D Particle - In - Cell code. *http://dx.doi.org/10.1051/proc:2007013*, 16, Jan. 2007.

[15] M. Griebel. The combination technique for the sparse grid solution of pde's on multiprocessor machines. *Parallel Process. Lett.*, 02(01):61–70, Mar. 1992. Publisher: World Scientific Publishing Co.

[16] M. Griebel. Adaptive sparse grid multilevel methods for elliptic PDEs based on finite differences. *Computing*, 61(2):151–179, June 1998.

[17] C. Guillet. Semi-implicit particle-in-cell methods embedding sparse grid reconstructions. *Submitted to SIAM:MMS*, 2023.

[18] A. Langdon. Effects of the spatial grid in simulation plasmas. *Journal of Computational Physics*, 6(2):247–267, Oct. 1970.

[19] B. Lo, V. Minden, and P. Colella. A real-space Green's function method for the numerical solution of Maxwell's equations. *Communications in Applied Mathematics and Computational Science*, 11(2):143–170, 2016.

[20] S. Muralikrishnan, A. J. Cerfon, M. Frey, L. F. Ricketson, and A. Adelmann. Sparse grid-based adaptive noise reduction strategy for particle-in-cell schemes. *Journal of Computational Physics: X*, 11:100094, June 2021.

[21] L. F. Ricketson and A. J. Cerfon. Sparse grid techniques for particle-in-cell schemes. *Plasma Phys. Control. Fusion*, 59(2):024002, Feb. 2017.

[22] E. Sonnendrücker. Monte carlo methods with applications to plasma physics. 2014.

[23] R. D. Sydora. Low-noise electromagnetic and relativistic particle-in-cell plasma simulation models. *Journal of Computational and Applied Mathematics*, 109(1):243–259, Sept. 1999.

Appendix

A Explicitation of constants

We provide here the constants K_E, D_E, K_ρ, D_ρ appearing in the Theorems 3.1 and 3.2. For $d = 3$, the constants for the electric field are:

$$K_E = K_1\|\partial_1^p\partial_2^p\partial_3^p\mathbf{E}\|_\infty + K_2\|\partial_1^{p+2}\partial_2^{p+2}\partial_3^{p+2}\mathbf{E}\|_\infty + K_3\|\partial_1^p\partial_2^p\partial_3^p\boldsymbol{\nabla}\rho\|_\infty + \sum_{i\neq j\neq k}\Big[K_4\|\partial_i^{p+1}\partial_j^{p+2}\partial_k^{p+2}\mathbf{E}\|_\infty$$
$$+ K_5\|\partial_i^p\partial_j^{p+1}\partial_k^{p+2}\mathbf{E}\|_\infty + K_6\|\partial_i^p\partial_j^{p+2}\partial_k^{p+2}\boldsymbol{\nabla}\rho\|_\infty + K_7\|\partial_i^p\partial_j^{p+2}\partial_k^{p+2}\mathbf{E}\|_\infty + K_8\|\partial_i^p\partial_j^p\partial_k^{p+2}\boldsymbol{\nabla}\rho\|_\infty$$
$$+ K_9\|\partial_i^p\partial_j^p\partial_k^{p+2}\mathbf{E}\|_\infty + K_{10}\|\partial_i^p\partial_j^p\partial_k^{p+1}\boldsymbol{\nabla}\rho\|_\infty\Big] + K_{11}\max_{i\neq j\neq k}\|\partial_i^p\partial_j^p\partial_k^{p+1}\Phi\|_\infty,$$
$$D_E = D_1(\mathcal{Q}\|\boldsymbol{\nabla}\rho\|_\infty)^{\frac{1}{2}},$$

where:

$$K_1 = C_{comb}C_{int}^3,\quad K_2 = 6C_{comb}C_{max}^2C_{lap}^3,\quad K_3 = C_{comb}(C_{max}C_{bias}^3 + 3C_{max}C_{int}^2C_{bias} + 3C_{max}C_{int}C_{bias}^2),$$
$$K_4 = C_{comb}C_{max}^2C_{lap}^2C_{grad},\quad K_5 = C_{comb}C_{max}C_{grad}C_{int}C_{lap}$$
$$K_6 = C_{comb}C_{max}^2C_{bias}C_{lap}^2,\quad K_7 = C_{comb}C_{max}C_{int}C_{lap}^2,$$
$$K_8 = C_{comb}(C_{max}^2C_{bias}^2C_{lap} + C_{max}^2C_{bias}C_{int}C_{lap}),\quad K_9 = C_{comb}C_{int}^2C_{max}C_{lap},$$
$$K_{10} = C_{comb}(C_{max}C_{grad}C_{bias}^2 + C_{max}C_{grad}C_{bias}C_{int}),\quad K_{11} = C_{comb}C_{int}^2C_{grad},$$
$$D_1 = (C_{comb}C_{max}C_{part}^3)^{\frac{1}{2}}.$$

For $d = 3$, the constants for the charge density are:

$$K_\rho = K_1\|\partial_1^p\partial_2^p\partial_3^p\rho\|_\infty,\quad K_1 = C_{comb}(C_{bias}^3 + 3C_{bias}^2C_{int} + 3C_{bias}C_{int}^2 + C_{int}^3),$$
$$D_\rho = D_1(\mathcal{Q}\|\rho\|_\infty)^{\frac{1}{2}},\quad D_1 = \left(\frac{36(21 + 4\log(2))}{\log(2)^2}\right)^{\frac{1}{2}}.$$

For $d = 2$, the constants for the electric field are:

$$K_E = K_1\|\partial_1^p\partial_2^p\mathbf{E}\|_\infty + K_2\|\partial_1^{p+2}\partial_2^{p+2}\mathbf{E}\|_\infty + K_3\|\partial_1^p\partial_2^p\boldsymbol{\nabla}\rho\|_\infty + \sum_{i\neq j}\Big[K_4\|\partial_i^{p+1}\partial_j^{p+2}\mathbf{E}\|_\infty$$
$$+ K_5\|\partial_i^p\partial_j^{p+2}\mathbf{E}\|_\infty + K_6\|\partial_i^p\partial_j^{p+2}\boldsymbol{\nabla}\rho\|_\infty + K_7\|\partial_i^p\partial_j^{p+1}\boldsymbol{\nabla}\rho\|_\infty\Big] + K_8\max_{i\neq j}\|\partial_i^p\partial_j^{p+1}\Phi\|_\infty,$$
$$D_E = D_1(\mathcal{Q}\|\boldsymbol{\nabla}\rho\|_\infty)^{\frac{1}{2}},$$

where:

$$K_1 = C_{comb}C_{int}^2,\quad K_2 = 2C_{comb}C_{max}^2C_{lap}^2,\quad K_3 = C_{comb}(C_{max}C_{bias}^2 + 2C_{max}C_{int}C_{bias}),$$
$$K_4 = C_{comb}C_{max}C_{lap}C_{grad},\quad K_5 = C_{comb}C_{max}C_{int}C_{lap},\quad K_6 = C_{comb}C_{max}C_{bias}C_{lap},$$
$$K_7 = C_{comb}C_{max}C_{grad}C_{bias},\quad K_8 = C_{comb}C_{int}C_{grad},\quad D_1 = (C_{comb}C_{max}C_{part}^2)^{\frac{1}{2}}.$$

For $d = 2$, the constants for the charge density are:

$$K_\rho = K_1\|\partial_1^p\partial_2^p\rho\|_\infty,\quad K_1 = C_{comb}(C_{bias}^2 + 2C_{bias}C_{int}^2 + C_{int}^2),$$
$$D_\rho = D_1(\mathcal{Q}\|\rho\|_\infty)^{\frac{1}{2}},\quad D_1 = \frac{4}{\log(2)}.$$

B Proofs of Lemmas 3.5, 3.6, 3.7, 3.8, 3.9.

The Lemmas are proved for the order $p = 4$. Results with $p = 2$ can be found in [6].

Proof of Lemma 3.5. Let us consider the one-dimensional case which can be extended to the d-

dimensional case by tensor product of the shape functions.

$$\mathbb{E}(\hat{\rho}_{h_l}(x)) = \mathcal{Q} \iint_{[-h_l^{-1},h_l^{-1}]\times\Omega_v} W(y) f(x+yh_l, v) dv, \tag{71}$$

$$= \sum_{\alpha\leq 4} h_l^\alpha \left(\int_{-2}^{2} W(y) y^\alpha dy\right) \left(\mathcal{Q}\int_{\Omega_v} \frac{\partial^\alpha f(x,v)}{\alpha!} dv\right) + o\big(h_l^4\big)\,, \tag{72}$$

where the change of variable $y = h_l^{-1}(\xi - x)$ and a Taylor expansion up to order 4 have been applied. The terms with odd exponent α vanish thanks to symmetry of the shape functions W, as well as the second order term owing to:

$$\int_{-2}^{2} W(y) y^2 dy = 2\left[\int_0^1 W(y) y^2 dy + \int_1^2 W(y) y^2 dy\right] = 2\left[\frac{11}{120} - \frac{11}{120}\right] = 0. \tag{73}$$

Eventually, we obtain the grid-based error result owing to the following relation:

$$\int_{-2}^{2} W(y) y^4 dy = 2\left[\int_0^1 W(y) y^4 dy + \int_1^2 W(y) y^4 dy\right] = 2\left[\frac{61}{1680} + \frac{13229}{1120}\right] = \frac{5687}{240}. \tag{74}$$

As for the particle sampling error, the result is obtained by the equation (95) from the proof outlined in Lemma C.3 with $k = l$. □

Proof of Lemma 3.6. For all $k \in \{1, ..., d\}$ such that $k \notin \{i_1, ..., i_m\}$, since $u \in \mathcal{C}^6(\Omega_{h_1}^{(i_1,\dots,i_m)})$, Taylor expansions in dimension k give the relations: $\forall \mathbf{j} \in \mathbf{I}_{h_1}$,

$$\Delta_{h_{l_k}} u(\mathbf{j}h_1) = \frac{16(u((\mathbf{j}+\mathbf{e}_k)h_1) + u((\mathbf{j}-\mathbf{e}_k)h_1)) - (u((\mathbf{j}+2\mathbf{e}_k)h_1) + u((\mathbf{j}-2\mathbf{e}_k)h_1)) - 30u(\mathbf{j}h_1)}{12h_{l_k}^2}$$

$$= \partial_k^2 u(\mathbf{j}h_1) - \frac{1}{90}\partial_k^6 u(\mathbf{j}h_1) h_{l_k}^4 + O\big(h^5\big)\,.$$

We obtain the result by summing upon the dimensions k. The same holds for each dimension of the gradient operator:

$$\nabla_{h_{l_k}} u(\mathbf{j}h_1) = \frac{8(u((\mathbf{j}+\mathbf{e}_k)h_1) + u((\mathbf{j}-\mathbf{e}_k)h_1)) - (u((\mathbf{j}+2\mathbf{e}_k)h_1) + u((\mathbf{j}-2\mathbf{e}_k)h_1))}{12h_{l_k}}$$

$$= \partial_k u(\mathbf{j}h_1) + \frac{2}{5}\partial_k^5 u(\mathbf{j}h_1) h_{l_k}^4 + O\big(h^5\big)\,. \square$$

Proof of Lemma 3.7. The proof is provided in [6].

Proof of Lemma 3.8. Let $\mathbf{x} \in \Omega_{h_l}^{(i_1,\dots,i_m)}$, the following holds true owing to the partition of unit property of the basis functions:

$$\mathcal{I}_{V_{h_l}} f(\mathbf{x}) - f(\mathbf{x}) = \sum_{\mathbf{j}\in\mathbf{I}_{h_1}} (f(\mathbf{j}h_1) - f(\mathbf{x})) W_{h_1,\mathbf{j}}(\mathbf{x}) \tag{75}$$

Let us introduce the notation $(y_{l_1,j_1}, \dots, y_{l_d,j_d}) \in \mathbb{R}^d$ defined by:

$$\mathbf{j}h_l - \mathbf{x} = (y_{l_1,j_1}, \dots, y_{l_d,j_d}) h_{\mathbf{1}}, \quad y_{l_k,j_k} = \begin{cases} j_k - \frac{x_k}{h_{l_k}} & \text{if } k \notin \{i_1, \dots, i_m\}, \\ 0 & \text{else.} \end{cases}$$

Because of the support of the basis functions:

$$|W_{h_l,\mathbf{j}}(\mathbf{x})| = 0 \Leftrightarrow \max(|y_{l_1,j_1}|, \dots, |y_{l_d,j_d}|) \geq p/2,$$

and the sum in equation (75) falls down to fifty four terms verifying $\max(|y_{l_1,j_1}|, \dots, |y_{l_d,j_d}|) < p/2$. Let $k \in [\![1, \dots, d-m]\!]$ and $r_1, \dots, r_k$ such that $\{r_1, \dots, r_k\} \subset \{1, \dots, d\}$ and $\{r_1, \dots, r_k\} \cap$

$\{i_1, \dots, i_m\} = \emptyset$, then a Taylor expansion of f in dimensions $r_1, \dots, r_k$ gives the relation:

$$f(\mathbf{j}h_\mathbf{l}) = \sum_{\substack{\boldsymbol{\alpha} \in \mathbb{N}^k \\ |\boldsymbol{\alpha}|_\infty \leq p}} \frac{\partial_{r_1}^{\alpha_1} \dots \partial_{r_k}^{\alpha_k} f(\mathbf{x})}{\boldsymbol{\alpha}!} y_{l_{r_1}, j_{r_1}}^{\alpha_1} \dots y_{l_{r_k}, j_{r_k}}^{\alpha_k} h_{l_{r_1}}^{\alpha_1} \dots h_{l_{r_k}}^{\alpha_k} + O(h_{l_{r_1}}^{p+1}, \dots, h_{l_{r_k}}^{p+1}).$$

because of the parity of basis functions, all the odd exponent vanishes. The exponent with value 2 also vanishes because of the cancellation of the q^{th} order moments for $q \in \{2k | 1 \leq k < p/2\}$ from the basis function construction:

$$\sum_{\mathbf{j} \in \mathbf{I}_{h_\mathbf{l}}} y_{l_{r_1}, j_{r_1}}^{\alpha_1} \dots y_{l_{r_k}, j_{r_k}}^{\alpha_k} W_{h_l, \mathbf{j}} = 0 \quad \text{if } \exists i \in \{1, \dots, k\} \quad \text{s.t. } \alpha_i \text{ odd. or } \alpha_i = q \forall q \in \{2k | 1 \leq k < p/2\}$$

The first result follows with:

$$d_{i_1, \dots, i_m; r_1, \dots, r_k} = p^{-k} \partial_{r_1}^p \dots \partial_{r_k}^p f \sum_{\mathbf{j} \in \mathbf{I}_{h_\mathbf{l}}} y_{l_{r_1}, j_{r_1}}^p \dots y_{l_{r_k}, j_{r_k}}^p W_{h_l, \mathbf{j}} + O(h_{l_{r_1}}^p, \dots, h_{l_{r_k}}^p),$$

where the sum can be recast into:

$$\begin{aligned}
\sum_{\mathbf{j} \in \mathbf{I}_{h_\mathbf{l}}} y_{l_{r_1}, j_{r_1}}^p \dots y_{l_{r_k}, j_{r_k}}^p W_{h_l, \mathbf{j}} =& y_{l_{r_1}, j_{r_1}}^p \dots y_{l_{r_k}, j_{r_k}}^p W^p(y_{l_{r_1}, j_{r_1}}) \dots W^p(y_{l_{r_k}, j_{r_k}}) \\
&+ y_{l_{r_1}, j_{r_1}}^p \dots (p/2 - 1 - y_{l_{r_k}, j_{r_k}})^p W^p(y_{l_{r_1}, j_{r_1}}) \dots W^p(y_{l_{r_{k-1}}, j_{r_{k-1}}}) W^p(p/2 - 1 - y_{l_{r_k}, j_{r_k}}) \\
&+ \dots \\
&+ y_{l_{r_1}, j_{r_1}}^p \dots (y_{l_{r_k}, j_{r_k}} - p/2)^p W^p(y_{l_{r_1}, j_{r_1}}) \dots W^p(y_{l_{r_{k-1}}, j_{r_{k-1}}}) W^p(y_{l_{r_k}, j_{r_k}} - p/2) \\
&+ \dots \\
&+ (p/2 - y_{l_{r_1}, j_{r_1}})^p \dots (p/2 - y_{l_{r_k}, j_{r_k}})^p W^p(p/2 - y_{l_{r_1}, j_{r_1}}) \dots W^p(p/2 - y_{l_{r_k}, j_{r_k}})
\end{aligned}$$

For $p = 4$ we can compute boundary for the previous function and the following estimation holds:

$$\left| \sum_{\mathbf{j} \in \mathbf{I}_{h_\mathbf{l}}} y_{l_{r_1}, j_{r_1}}^2 \dots y_{l_{r_k}, j_{r_k}}^2 W_{h_l, \mathbf{j}} \right| \leq (2.(0.089) + 2.(0.381))^k \leq 4^k (0.237)^k$$

which gives the results.

Proof of Lemma 3.9. The proof for $p = 4, 6$ is the same as the one for $p = 2$ which can be found in [15].

C Proof of Theorem 3.2

C.1 Definitions and Lemmas

Regarding the particle sampling error estimate, our result is novel, offering a more precise bound compared to the one presented in [6]. The Theorem is proved for the order $p = 4$ and dimension $d = 3$. To establish this result, we introduce specific notations and Lemmas.

Definition C.1 *Let $\boldsymbol{k}, \boldsymbol{l} \in \mathbb{N}^3$, $0 \leq r \leq s \leq 2$, we introduce the notations:*

$$\boldsymbol{k}^{r,s} = (k_r, ..., k_s) \in \mathbb{N}^{s-r+1}, \quad (\boldsymbol{k}, \boldsymbol{l})^{r,s} = (k_r, ..., k_s, l_r, ..., l_s) \in (\mathbb{N}^{s-r+1})^2, \tag{76}$$

$$|\boldsymbol{k}|_1^{r,s} = \sum_{i=r}^{s} |k_i|, \tag{77}$$

and the index set:

$$\mathbb{I}_n^r := [\![1, n]\!]^r. \tag{78}$$

By introducing the spaces:

$$\mathbb{F}_n^r := \{(\boldsymbol{k},\boldsymbol{l}) \in \mathbb{I}_n^r \times \mathbb{I}_n^r \mid k_m = l_m,\ m \in [\![1,...,r]\!]\}, \tag{79}$$
$$\mathbb{G}_n^r := \{(\boldsymbol{k},\boldsymbol{l}) \in \mathbb{I}_n^r \times \mathbb{I}_n^r \mid k_m < l_m,\ m \in [\![1,...,r]\!]\}, \tag{80}$$
$$\mathbb{H}_n^r := \{(\boldsymbol{k},\boldsymbol{l}) \in \mathbb{I}_n^r \times \mathbb{I}_n^r \mid k_m > l_m,\ m \in [\![1,...,r]\!]\}, \tag{81}$$

the following decomposition of the index sets holds:

$$\mathbb{I}_n^2 \times \mathbb{I}_n^2 = \bigcup_{0\le r\le s\le 2} \mathbb{F}_n^r \times \mathbb{G}_n^{s-r} \times \mathbb{H}_n^{2-s}, \tag{82}$$

By definition, it follows some equalities between the cardinal of the subspaces $|\mathbb{I}_n^r| = |\mathbb{F}_n^r| = O(n^r)$, $|\mathbb{G}_n^r| = |\mathbb{H}_n^r| = O\big(n^{2r}\big)$.

Definition C.2 *Let us introduce the notation for the interpolation in two variables of* Ω*, i.e. for a function* $f \in \Omega^2$*:*

$$\mathcal{I}_{V_{h_k},V_{h_l}} f(\boldsymbol{x},\boldsymbol{y}) = \sum_{\boldsymbol{i}\in\mathbf{I}_{h_k}} \sum_{\boldsymbol{j}\in\mathbf{I}_{h_l}} f(\boldsymbol{i}h_{\boldsymbol{k}},\boldsymbol{j}h_l) W_{h_k;\boldsymbol{i}} W_{h_l;\boldsymbol{j}}. \tag{83}$$

Lemma C.3 *Let* $\boldsymbol{k},\boldsymbol{l} \in \mathbb{L}_n$*, then*

$$\frac{\mathcal{Q}}{h_{\boldsymbol{k}} h_{\boldsymbol{l}}} \mathcal{I}_{V_{h_k},V_{h_l}} \mathbb{E}(W_{h_k}(\boldsymbol{x}-\boldsymbol{X}) W_{h_l}(\boldsymbol{y}-\boldsymbol{X})) \le \frac{\|\rho\|_\infty}{h_{\tilde{\boldsymbol{k}}}} + O\big(h_{\tilde{l}}\big) \tag{84}$$

where $\tilde{\boldsymbol{k}},\tilde{\boldsymbol{l}} \in \mathbb{N}^3$ *such that* $\tilde{k}_m = \min(k_m,l_m)$, $\tilde{l}_m = \max(k_m,l_m)$, $m = 1,2,3$.

Lemma C.4 *Let* $\boldsymbol{k},\boldsymbol{l} \in \mathbb{N}^3$ *and*

$$M(\boldsymbol{k},\boldsymbol{l}) = \frac{1}{h_{\tilde{k}_1}} \cdot \frac{1}{h_{\tilde{k}_2}} \cdot \frac{1}{h_{\tilde{k}_3}}, \tag{85}$$

where $\tilde{k}_m = \min(k_m,l_m)$, $m = 1,2,3$, *then the following bound holds true:*

$$\sum_{(\boldsymbol{k},\boldsymbol{l})\in(\mathbb{L}_n)^2} M(\boldsymbol{k},\boldsymbol{l}) \le 9 \sum_{(\boldsymbol{k},\boldsymbol{l})\in(\mathbb{L}_{n,0})^2} M(\boldsymbol{k},\boldsymbol{l}). \tag{86}$$

Lemma C.5 *Let* $\alpha \in \mathbb{N}^*$, $\beta \in [\![0,...,2]\!]$, $m > 0$ *then*

$$\sum_{\substack{(k,l)\in\mathbb{I}_n\times\mathbb{I}_n,\\ k<l}} h_{l-k}(l-k)^\beta = n(-1)^\beta \left(\frac{2^{-x}}{1-2^{-x}}\right)^{(\beta)}\Big|_{x=1} + O(1), \tag{87}$$

$$\sum_{\substack{(k,l)\in\mathbb{I}_n\times\mathbb{I}_n,\\ k<l}} h_{l-k}^\alpha = \frac{n}{1-2^{-\alpha}} + O(1), \tag{88}$$

$$\sum_{\substack{(k,l)\in\mathbb{I}_n\times\mathbb{I}_n,\\ l\le k-m}} h_{k-l} = 2nh_m + O(1). \tag{89}$$

C.2 Proofs of Lemmas C.3, C.4, C.5

Proof of Lemma C.3. Let us consider the one-dimensional case which can be extended to the d-dimensional case by tensor product of the shape functions and let us also assume that $l \ge k$ without

loss of generality, then owing to the symmetry of the basis functions, it holds:

$$\begin{aligned}
&\mathcal{Q}\mathbb{E}\Big(\frac{1}{h_k h_l} W_{h_k}(ih_k - X) W_{h_l}(jhl - X)\Big) \\
&\qquad = \mathcal{Q}\int_{\Omega_x\times\Omega_v} \frac{1}{h_k h_l} W\left(\frac{\xi - ih_k}{h_k}\right) W\left(\frac{\xi - jh_l}{h_l}\right) f(\xi, v, t) d\xi dv \\
&\qquad = \mathcal{Q}\int_{\Omega_x\times\Omega_v} \frac{1}{h_k} W\left(xh_{l-k} + jh_{l-k} - i\right) W\left(x\right) f(jh_l + xh_l, v, t) dx dv \\
&\qquad = \frac{\rho(jh_l)}{h_k}\int_{-\frac{1}{h_l}}^{\frac{1}{h_l}} W\left(xh_{l-k} + jh_{l-k} - i\right) W\left(x\right) dx + O(h_l)\,,
\end{aligned}$$

where the change of variable $x = h_l^{-1}(\xi - jh_l)$ and a Taylor expansion in f have been applied. The integral $\int_{-2}^{2} W(x)W(xh_{l-k} + jh_{l-k} - i)dx$ is different from 0 for i, j such that:

$$jh_{l-k} - i = -2 - h_{l-k}, -2, -2 + h_{l-k}, ..., -h_{l-k}, 0, h_{l-k}, ..., 2 - h_{l-k}, 2, 2 + h_{l-k}. \tag{90}$$

By considering and computing all the different cases, one can see that the integral is maximum for $jh_{l-k} - i = 0$. In that case, the integral falls down, by symmetry, to:

$$\int_{-2}^{2} W(x)W(xh_{l-k} + jh_{l-k} - i)dx = 2\Big(\int_{0}^{1} W(x)W(xh_{l-k} + jh_{l-k} - i)dx \tag{91}$$

$$+ \int_{1}^{2} W(x)W(xh_{l-k} + jh_{l-k} - i)dx\Big), \tag{92}$$

and

$$\int_{0}^{1} W(x)W(xh_{l-k} + jh_{l-k} - i)dx = \frac{13}{24} - \frac{11}{120}h_{l-k} - \frac{11}{120}h_{l-k}^2 + \frac{23}{840}h_{l-k}^3, \tag{93}$$

$$\int_{1}^{2} W(x)W(xh_{l-k} + jh_{l-k} - i)dx = -\frac{1}{24} + \frac{121}{1080}h_{l-k} - \frac{11}{120}h_{l-k}^2 + \frac{59}{2520}h_{l-k}^3. \tag{94}$$

Therefore, we have

$$\begin{aligned}
&\mathcal{Q}\mathbb{E}\Big(\frac{1}{h_k h_l} W_{h_k}(ih_k - X) W_{h_l}(jhl - X)\Big) = \\
&\quad \frac{\rho(jh_l)}{h_k}\left(1 + \frac{11}{270}h_{l-k} - \frac{44}{120}h_{l-k}^2 + \frac{32}{315}h_{l-k}^3\right) + O(h_l) \leq \frac{\|\rho\|_\infty}{h_k} + O(h_l)\,,
\end{aligned} \tag{95}$$

since the maximum on $[0, 1]$ of the function $P(x) = 1 + \frac{11}{270}x - \frac{44}{120}x^2 + \frac{32}{315}x^3$ is obtained for $x = 0$.

Eventually, using the partition of unit property of the basis function:

$$\frac{\mathcal{Q}}{h_k h_l}\mathcal{I}_{V_{h_k}, V_{h_l}}\mathbb{E}(W_{h_k}(x - X)W_{h_l}(y - X)) \leq \frac{\|\rho\|_\infty}{h_k} + O(h_l)\,. \ \square$$

Proof of Lemma C.4. Let us recall that:

$$\mathbb{L}_n := \bigcup_{i\in[\![0,2]\!]} \mathbb{L}_{n,i}, \quad \mathbb{L}_{n,i} := \{\mathbf{l} \in \mathbb{N}^3 \mid |\mathbf{l}|_1 = n + 2 - i,\ \mathbf{l} \geq \mathbf{1}\}, \tag{96}$$

and let $i \in \{0, 1\}$, so that we have:

$$\forall \mathbf{l} \in \mathbb{L}_{n,i+1},\ \exists \tilde{\mathbf{l}} \in \mathbb{L}_{n,i} \ \text{ and } \ \exists \tilde{j} \in \{1, 2, 3\} \ s.t.\ \tilde{l}_j = l_j,\ j \neq \tilde{j} \ \text{ and } \ \tilde{l}_{\tilde{j}} > l_{\tilde{j}}. \tag{97}$$

It follows that $M(\mathbf{k},\mathbf{l}) \leq M(\mathbf{k},\tilde{\mathbf{l}})$ for any $\mathbf{k} \in \mathbb{L}_n$ and thus:

$$\begin{aligned}
\sum_{(\mathbf{k},\mathbf{l})\in(\mathbb{L}_n)^2} M(\mathbf{k},\mathbf{l}) &= \sum_{i=0}^{2}\sum_{j=0}^{2}\sum_{\mathbf{k}\in\mathbb{L}_{n,i}}\sum_{\mathbf{l}\in\mathbb{L}_{n,j}} M(\mathbf{k},\mathbf{l}) \\
&= \sum_{(\mathbf{k},\mathbf{l})\in(\mathbb{L}_{n,0})^2} M(\mathbf{k},\mathbf{l}) + \sum_{\mathbf{k}\in\mathbb{L}_{n,0}}\sum_{\mathbf{l}\in\mathbb{L}_{n,1}} M(\mathbf{k},\mathbf{l}) \sum_{\mathbf{k}\in\mathbb{L}_{n,1}}\sum_{\mathbf{l}\in\mathbb{L}_{n,1}} M(\mathbf{k},\mathbf{l}) + ... \\
&\leq \sum_{(\mathbf{k},\mathbf{l})\in(\mathbb{L}_{n,0})^2} M(\mathbf{k},\mathbf{l}) + \sum_{\mathbf{k}\in\mathbb{L}_{n,0}}\sum_{\mathbf{l}\in\mathbb{L}_{n,0}} M(\mathbf{k},\mathbf{l}) \sum_{\mathbf{k}\in\mathbb{L}_{n,1}}\sum_{\mathbf{l}\in\mathbb{L}_{n,0}} M(\mathbf{k},\mathbf{l}) + ... \\
&\leq ... \leq 9 \sum_{(\mathbf{k},\mathbf{l})\in(\mathbb{L}_{n,0})^2} M(\mathbf{k},\mathbf{l}). \ \square
\end{aligned}$$

Proof of Lemma C.5. Let $\beta \in [\![0,...,d-1]\!]$, then:

$$\begin{aligned}
\sum_{\substack{(k,l)\in\mathbb{I}_n\times\mathbb{I}_n,\\ k<l}} h_{l-k}(l-k)^\beta &= \sum_{l=1}^{n}\sum_{k=1}^{l-1} k^\beta 2^{-k} = \sum_{l=1}^{n}(-1)^\beta \left(\frac{2^{-x}}{1-2^{-x}}\left(1-2^{-(l-1)x}\right)\right)^{(\beta)}\Big|_{x=1} \\
&= \sum_{l=1}^{n}(-1)^\beta \left(\sum_{m=0}^{\beta}\binom{\beta}{m}\left(\frac{2^{-x}}{1-2^{-x}}\right)^{(\beta-m)}\left(1-2^{-(l-1)x}\right)^{(m)}\right)\Big|_{x=1} \\
&= \sum_{l=1}^{n}(-1)^\beta \left(\left(\frac{2^{-x}}{1-2^{-x}}\right)^{(\beta)}\left(1-2^{-(l-1)x}\right)\right. \\
&\quad \left. + \sum_{m=1}^{\beta}\binom{\beta}{m}\left(\frac{2^{-x}}{1-2^{-x}}\right)^{(\beta-m)}(-1)^{m+1}(l-1)^m 2^{-(l-1)x}\right)\Big|_{x=1} \\
&= \sum_{l=1}^{n}\left((-1)^\beta\left(\left(\frac{2^{-x}}{1-2^{-x}}\right)^{(\beta)}\right)\Big|_{x=1} + O(2^{-l})\right) \\
&= n(-1)^\beta\left(\frac{2^{-x}}{1-2^{-x}}\right)^{(\beta)}\Big|_{x=1} + O(1)\,.
\end{aligned}$$

Let $\alpha \in [\![1,...,d-1]\!]$, then:

$$\begin{aligned}
\sum_{\substack{(k,l)\in\mathbb{I}_n\times\mathbb{I}_n,\\ k<l}} h_{l-k}^\alpha &= \sum_{l=1}^{n} 2^{-\alpha l}\sum_{k=1}^{l-1} 2^{\alpha k} = \sum_{l=1}^{n} 2^{-\alpha l}\frac{2^\alpha}{2^\alpha-1}(2^{\alpha(l-1)}-1) \\
&= \frac{n}{2^\alpha-1} - \frac{1-2^{\alpha n}}{(2^\alpha-1)(1-2^{-\alpha})}.
\end{aligned}$$

Let $m > 0$, then:

$$\sum_{\substack{(k,l)\in\mathbb{I}_n\times\mathbb{I}_n,\\ l\leq k-m}} h_{k-l} = \sum_{k=1}^{n} 2^{-k}\sum_{l=1}^{k-m} 2^l = 2nh_m - (1-2^{-n}). \ \square$$

Proof of Theorem 3.2. The outcome concerning grid-based errors is achieved through the straightforward application of the projection (3.5), interpolation (3.8), and recombination (3.9) Lemmas. For the particle sampling error, by linearity, the following bound for the variance of the reconstructed

charge density holds true:

$$\mathbb{V}\left(\mathcal{V}(\hat{\rho}^c_{h_n})\right) = \mathbb{V}\left(\hat{\rho}^c_{h_n} - \mathbb{E}(\hat{\rho}^c_{h_n})\right) \tag{98}$$

$$= \mathbb{V}\left(\sum_{\mathbf{l}\in\mathbb{L}_n} c_{\mathbf{l}}\mathcal{I}_{V_{h_\mathbf{l}}}\hat{\rho}_{h_\mathbf{l}} - \sum_{\mathbf{l}\in\mathbb{L}_n} c_{\mathbf{l}}\mathcal{I}_{V_{h_\mathbf{l}}}\mathbb{E}(\hat{\rho}_{h_\mathbf{l}})\right) \tag{99}$$

$$= \mathbb{V}\left(\sum_{\mathbf{l}\in\mathbb{L}_n} c_{\mathbf{l}}\mathcal{I}_{V_{h_\mathbf{l}}}\mathcal{V}(\hat{\rho}_{h_\mathbf{l}})\right) \tag{100}$$

$$\leq \sum_{(\mathbf{k},\mathbf{l})\in(\mathbb{L}_n)^2} |c_\mathbf{k}||c_\mathbf{l}| \left|\mathrm{Cov}(\mathcal{I}_{V_{h_\mathbf{k}}}\mathcal{V}(\hat{\rho}_{h_\mathbf{k}}), \mathcal{I}_{V_{h_\mathbf{l}}}\mathcal{V}(\hat{\rho}_{h_\mathbf{l}}))\right|. \tag{101}$$

First, let us have a look at the covariance of the pairs ($\mathbf{k}$ and $\mathbf{l}$) of component grids:

$$\begin{aligned}\mathrm{Cov}(\mathcal{I}_{V_{h_\mathbf{k}}}\mathcal{V}(\hat{\rho}_{h_\mathbf{k}}), \mathcal{I}_{V_{h_\mathbf{l}}}\mathcal{V}(\hat{\rho}_{h_\mathbf{l}})) &= \mathbb{E}(\mathcal{I}_{V_{h_\mathbf{k}}}\mathcal{V}(\hat{\rho}_{h_\mathbf{k}})\mathcal{I}_{V_{h_\mathbf{l}}}\mathcal{V}(\hat{\rho}_{h_\mathbf{l}})) - \mathbb{E}(\mathcal{I}_{V_{h_\mathbf{k}}}\mathcal{V}(\hat{\rho}_{h_\mathbf{k}}))\mathbb{E}(\mathcal{I}_{V_{h_\mathbf{l}}}\mathcal{V}(\hat{\rho}_{h_\mathbf{l}})) \\ &= \mathbb{E}(\mathcal{I}_{V_{h_\mathbf{k}}}\mathcal{V}(\hat{\rho}_{h_\mathbf{k}})\mathcal{I}_{V_{h_\mathbf{l}}}\mathcal{V}(\hat{\rho}_{h_\mathbf{l}})) - \mathcal{I}_{V_{h_\mathbf{k}}}\mathbb{E}(\mathcal{V}(\hat{\rho}_{h_\mathbf{k}}))\mathcal{I}_{V_{h_\mathbf{l}}}\mathbb{E}(\mathcal{V}(\hat{\rho}_{h_\mathbf{l}})). \\ &= \mathbb{E}(\mathcal{I}_{V_{h_\mathbf{k}}}\mathcal{V}(\hat{\rho}_{h_\mathbf{k}})\mathcal{I}_{V_{h_\mathbf{l}}}\mathcal{V}(\hat{\rho}_{h_\mathbf{l}})),\end{aligned}$$

since the random variables $\mathcal{V}(\hat{\rho}_{h_\mathbf{l}})$ and $\mathcal{V}(\hat{\rho}_{h_\mathbf{k}})$ are centered. By linearity of the expected value, it follows:

$$\begin{aligned}\mathrm{Cov}(\mathcal{I}_{V_{h_\mathbf{k}}}\mathcal{V}(\hat{\rho}_{h_\mathbf{k}}), \mathcal{I}_{V_{h_\mathbf{l}}}\mathcal{V}(\hat{\rho}_{h_\mathbf{l}})) &= \mathcal{I}_{V_{h_\mathbf{k}},V_{h_\mathbf{l}}}\mathbb{E}(\mathcal{V}(\hat{\rho}_{h_\mathbf{k}})\mathcal{V}(\hat{\rho}_{h_\mathbf{l}})) \\ &= \mathcal{I}_{V_{h_\mathbf{k}},V_{h_\mathbf{l}}}\left(\mathbb{E}(\hat{\rho}_{h_\mathbf{k}}\hat{\rho}_{h_\mathbf{l}}) - \mathbb{E}(\hat{\rho}_{h_\mathbf{k}})\mathbb{E}(\hat{\rho}_{h_\mathbf{l}})\right).\end{aligned}$$

We have:

$$\begin{aligned}\mathbb{E}(\hat{\rho}_{h_\mathbf{k}}\hat{\rho}_{h_\mathbf{l}}) &= \frac{\mathcal{Q}^2}{N^2}\frac{1}{h_\mathbf{k}h_\mathbf{l}}\sum_{p,q=1}^{N}\mathbb{E}\left(W_{h_\mathbf{k}}(\mathbf{x}-\mathbf{X}_p)W_{h_\mathbf{l}}(\mathbf{y}-\mathbf{X}_q)\right) \\ &= \frac{\mathcal{Q}^2}{N^2}\frac{1}{h_\mathbf{k}h_\mathbf{l}}\Big(\sum_{p=1}^{N}\mathbb{E}\left(W_{h_\mathbf{k}}(\mathbf{x}-\mathbf{X}_p)W_{h_\mathbf{l}}(\mathbf{y}-\mathbf{X}_p)\right) + \sum_{\substack{p,q=1\\p\neq q}}^{N}\mathbb{E}\left(W_{h_\mathbf{k}}(\mathbf{x}-\mathbf{X}_p)\right)\mathbb{E}\left(W_{h_\mathbf{l}}(\mathbf{y}-\mathbf{X}_q)\right)\Big) \\ &= \frac{\mathcal{Q}^2}{N^2}\frac{1}{h_\mathbf{k}h_\mathbf{l}}\Big(N\mathbb{E}\left(W_{h_\mathbf{k}}(\mathbf{x}-\mathbf{X})W_{h_\mathbf{l}}(\mathbf{y}-\mathbf{X})\right) + N(N-1)\mathbb{E}\left(W_{h_\mathbf{k}}(\mathbf{x}-\mathbf{X})\right)\mathbb{E}\left(W_{h_\mathbf{l}}(\mathbf{y}-\mathbf{X})\right)\Big),\end{aligned}$$

since the random variables $\mathbf{X}_p$ are i.i.d and by independency of the random variables $\mathbf{X}_p$ and $\mathbf{X}_q$ when $p \neq q$, and:

$$\mathbb{E}(\hat{\rho}_{h_\mathbf{k}})\mathbb{E}(\hat{\rho}_{h_\mathbf{l}}) = \frac{\mathcal{Q}^2}{h_\mathbf{k}h_\mathbf{l}}\mathbb{E}\left(W_{h_\mathbf{k}}(\mathbf{x}-\mathbf{X})\right)\mathbb{E}\left(W_{h_\mathbf{l}}(\mathbf{y}-\mathbf{X})\right)$$

From these expressions, one gets:

$$\mathrm{Cov}(\mathcal{I}_{V_{h_\mathbf{k}}}\mathcal{V}(\hat{\rho}_{h_\mathbf{k}}), \mathcal{I}_{V_{h_\mathbf{l}}}\mathcal{V}(\hat{\rho}_{h_\mathbf{l}})) = \frac{\mathcal{Q}^2}{N}\frac{1}{h_\mathbf{k}h_\mathbf{l}}\mathcal{I}_{V_{h_\mathbf{k}},V_{h_\mathbf{l}}}\mathbb{E}(W_{h_\mathbf{k}}(\mathbf{x}-\mathbf{X})W_{h_\mathbf{l}}(\mathbf{y}-\mathbf{X})) + O\left(\frac{1}{N}\right),$$

where we use the result:

$$h_\mathbf{k}^{-1}\mathbb{E}(W_{h_\mathbf{k}}(\mathbf{x}-\mathbf{X})) = O(1). \tag{102}$$

Note that the first term scales as $O\big((h_\mathbf{l}h_\mathbf{k}N)^{-1}\big)$ and is dominant in comparison to the negligible term (in $O\big(N^{-1}\big)$). On the other hand, according to Lemmas C.3 and C.4, the sum of the component

grid pairs of covariance is bound by the sum on the more refined grids:

$$\begin{aligned}\mathbb{V}\left(\mathcal{V}(\hat{\rho}^c_{h_n})\right) &\leq 9 \max_{\mathbf{l}\in\mathbb{L}_n} |c_{\mathbf{l}}|^2 \sum_{\substack{(\mathbf{k},\mathbf{l})\in(\mathbb{N}^*)^6,\\ |\mathbf{k}|_1=n+2,\\ |\mathbf{l}|_1=n+2,}} \left(\left|\mathrm{Cov}(\mathcal{I}_{V_{h_{\mathbf{k}}}}\mathcal{V}(\hat{\rho}_{h_{\mathbf{k}}}), \mathcal{I}_{V_{h_{\mathbf{l}}}}\mathcal{V}(\hat{\rho}_{h_{\mathbf{l}}}))\right| + O\left(\frac{1}{N}\right)\right) \\ &\leq 36 \sum_{(\mathbf{k},\mathbf{l})\in\mathbb{I}^2_n\times\mathbb{I}^2_n} \left|\mathrm{Cov}(\mathcal{I}_{V_{h_{\mathbf{k}^\star}}}\mathcal{V}(\hat{\rho}_{h_{\mathbf{k}^\star}}), \mathcal{I}_{V_{h_{\mathbf{l}^\star}}}\mathcal{V}(\hat{\rho}_{h_{\mathbf{l}^\star}}))\right|,\end{aligned}$$

where the negligible term has been omitted and:

$$\mathbf{k}^\star := (\mathbf{k}, n+2-|\mathbf{k}|_1), \quad \mathbf{l}^\star := (\mathbf{l}, n+2-|\mathbf{l}|_1). \tag{103}$$

The conditions on the l^1-norms of the grid levels reduce the degrees of freedom from 6 to 4. Let us now consider all different configurations of component grid pairs, *i.e.* if $k_m = l_m$ or $k_m < l_m$ or $k_m > l_m$, for $m = 1, ..., d-1$. The sum can be recast into:

$$\begin{aligned}&\sum_{(\mathbf{k},\mathbf{l})\in\mathbb{I}^2_n\times\mathbb{I}^2_n} \left|\mathrm{Cov}(\mathcal{I}_{V_{h_{\mathbf{k}^\star}}}\mathcal{V}(\hat{\rho}_{h_{\mathbf{k}^\star}}), \mathcal{I}_{V_{h_{\mathbf{l}^\star}}}\mathcal{V}(\hat{\rho}_{h_{\mathbf{l}^\star}}))\right| \\ &\qquad = \sum_{0\leq r\leq s\leq 2} \binom{r}{2}\binom{s-r}{2} \sum_{\substack{(\mathbf{k},\mathbf{l})\in\mathbb{F}^r_n\times\\ \mathbb{G}^{s-r}_n\times\mathbb{H}^{2-s}_n}} \left|\mathrm{Cov}(\mathcal{I}_{V_{h_{\mathbf{k}^\star}}}\mathcal{V}(\hat{\rho}_{h_{\mathbf{k}^\star}}), \mathcal{I}_{V_{h_{\mathbf{l}^\star}}}\mathcal{V}(\hat{\rho}_{h_{\mathbf{l}^\star}}))\right|.\end{aligned}$$

Let $0 \leq r \leq s \leq 2$ be integers, and let us consider the innermost sum of the last expression. The r first components are such that $k_m = l_m$, $m = 1, ..., r$. Then, the $s-r$ following are such that $k_m < l_m$, $m = r+1, ..., s$ and finally the last $2-s$ components are such that $k_m > l_m$, $m = s+1, ..., 2$. Two cases are to distinguish, either if $k^\star_3 > l^\star_3$ or $k^\star_3 \leq l^\star_3$:
I) If $k^\star_3 > l^\star_3$: then $|\mathbf{k}|_1 < |\mathbf{l}|_1$ and $s > r$. It gives us three possible configurations separated into two cases:

I.i) If $s = 2$: then $r = 0$ or $r = 1$ and according to equation (84) of Lemma **??**, one gets the following bound:

$$\begin{aligned}&\sum_{\substack{(\mathbf{k},\mathbf{l})\in\mathbb{F}^r_n\times\\ \mathbb{G}^{2-r}_n}} \left|\mathrm{Cov}(\mathcal{I}_{V_{h_{\mathbf{k}^\star}}}\mathcal{V}(\hat{\rho}_{h_{\mathbf{k}^\star}}), \mathcal{I}_{V_{h_{\mathbf{l}^\star}}}\mathcal{V}(\hat{\rho}_{h_{\mathbf{l}^\star}}))\right| \\ &\leq \frac{\mathcal{Q}\|\rho\|_\infty}{N} \sum_{\substack{(\mathbf{k},\mathbf{l})\in\mathbb{F}^r_n\times\\ \mathbb{G}^{2-r}_n}} \left[\frac{1}{h_{k_1}h_{k_2}}\frac{1}{h_{l^\star_3}} + O\big(h_{n+2}h_{|\mathbf{l}-\mathbf{k}|_1}\big)\right] \\ &\leq \frac{\mathcal{Q}\|\rho\|_\infty}{Nh_{n+2}} \sum_{\substack{(\mathbf{k},\mathbf{l})\in\\ \mathbb{F}^r_n\times\mathbb{G}^{2-r}_n}} \left[h_{|\mathbf{l}-\mathbf{k}|_1} + O\big(h_{n+2}h_{|\mathbf{l}-\mathbf{k}|_1}\big)\right] \\ &\leq \begin{cases} 4n^2\dfrac{\mathcal{Q}\|\rho\|_\infty}{Nh_{n+2}} + O\left(\dfrac{n^2}{N}\right) & \text{if } r=0, \\ 2n^2\dfrac{\mathcal{Q}\|\rho\|_\infty}{Nh_{n+2}} + O\left(\dfrac{n^2}{N}\right) & \text{if } r=1, \end{cases}\end{aligned}$$

where equation (88) of Lemma C.5 has been used for the last expression.

I.ii) If $s = 1$: then $r = 0$ and again according to equation (84) of Lemma C.3, the following bound

holds true:

$$\sum_{\substack{(\mathbf{k},\mathbf{l})\in\\ \mathbb{G}_n^1\times\mathbb{H}_n^1}} \Big|\mathrm{Cov}(\mathcal{I}_{V_{h_{\mathbf{k}^\star}}}\mathcal{V}(\hat{\rho}_{h_{\mathbf{k}^\star}}),\mathcal{I}_{V_{h_{\mathbf{l}^\star}}}\mathcal{V}(\hat{\rho}_{h_{\mathbf{l}^\star}}))\Big|$$
$$\leq \frac{\mathcal{Q}\|\rho\|_\infty}{N}\sum_{\substack{(\mathbf{k},\mathbf{l})\in\\ \mathbb{G}_n^1\times\mathbb{H}_n^1}}\Big[\frac{1}{h_{k_1}h_{l_2}}\frac{1}{h_{l_3^\star}}+O\Big(h_{n+2}h_{|\mathbf{l}-\mathbf{k}|_1^{1,1}}\Big)\Big]$$
$$\leq \frac{\mathcal{Q}\|\rho\|_\infty}{Nh_{n+2}}\sum_{(k_1,l_1)\in\mathbb{G}_n^1}\Bigg[\Big(h_{|\mathbf{l}-\mathbf{k}|_1^{1,1}}+O\Big(h_{n+2}h_{|\mathbf{l}-\mathbf{k}|_1^{1,1}}\Big)\Big)\Big(\sum_{\substack{(k_2,l_2)\in\mathbb{H}_n^1,\\ |\mathbf{k}|_1^{1,2}\leq|\mathbf{l}|_1^{1,2}}}1\Big)\Bigg].$$

In addition, for $\mathbf{k},\mathbf{l}\in\mathbb{N}^2$ such that $k_1<l_1$, the following bound is verified:

$$\sum_{\substack{(k_2,l_2)\in\mathbb{H}_n^1,\\ |\mathbf{k}|_1^{1,2}\leq|\mathbf{l}|_1^{1,2}}}1 \quad\leq\quad \sum_{\substack{l_2\in\mathbb{I}_n^1\\ k_2\in]\!]l_2,l_2+|\mathbf{l}-\mathbf{k}|_1^{1,1}]\!]}}1 \quad=\quad n|\mathbf{l}-\mathbf{k}|_1^{1,1}.$$

Then, according to equation (87) of Lemma C.5, the previous expression is bounded by:

$$\sum_{\substack{(\mathbf{k},\mathbf{l})\in\\ \mathbb{G}_n^1\times\mathbb{H}_n^1}} \Big|\mathrm{Cov}(\mathcal{I}_{V_{h_{\mathbf{k}^\star}}}\mathcal{V}(\hat{\rho}_{h_{\mathbf{k}^\star}}),\mathcal{I}_{V_{h_{\mathbf{l}^\star}}}\mathcal{V}(\hat{\rho}_{h_{\mathbf{l}^\star}}))\Big|$$
$$\leq \frac{n\mathcal{Q}\|\rho\|_\infty}{Nh_{n+2}}\sum_{(k_1,l_1)\in\mathbb{G}_n^1}\Big[h_{|\mathbf{l}-\mathbf{k}|_1^{1,1}}|\mathbf{l}-\mathbf{k}|_1^{1,1}+O\Big(h_{n+2}h_{|\mathbf{l}-\mathbf{k}|_1^{1,1}}|\mathbf{l}-\mathbf{k}|_1^{1,1}\Big)\Big]$$
$$\leq -\frac{n^2\mathcal{Q}\|\rho\|_\infty}{Nh_{n+2}}\frac{d}{dx}\left(\frac{2^{-x}}{1-2^{-x}}\right)_{|x=1}+O\Big(\frac{n^2}{N}\Big)\leq\frac{2\log(2)n^2\mathcal{Q}\|\rho\|_\infty}{Nh_{n+2}}+O\Big(\frac{n^2}{N}\Big)$$

II) If $k_3^\star\leq l_3^\star$: then $|\mathbf{l}|_1\leq|\mathbf{k}|_1$ and two cases are to consider:

II.i) If $s<2$: then, according to equation (84) of Lemma C.3, one gets the following bound:

$$\sum_{\substack{(\mathbf{k},\mathbf{l})\in\mathbb{F}_n^r\times\\ \mathbb{G}_n^{s-r}\times\mathbb{H}_n^{2-s}}} \Big|\mathrm{Cov}(\mathcal{I}_{V_{h_{\mathbf{k}^\star}}}\mathcal{V}(\hat{\rho}_{h_{\mathbf{k}^\star}}),\mathcal{I}_{V_{h_{\mathbf{l}^\star}}}\mathcal{V}(\hat{\rho}_{h_{\mathbf{l}^\star}}))\Big|$$
$$\leq \frac{\mathcal{Q}\|\rho\|_\infty}{N}\sum_{\substack{(\mathbf{k},\mathbf{l})\in\mathbb{F}_n^r\times\\ \mathbb{G}_n^{s-r}\times\mathbb{H}_n^{2-s}}}\frac{1}{h_{k_1}...h_{k_r}}\frac{1}{h_{k_{r+1}}...h_{k_s}}\frac{1}{h_{l_{s+1}}...h_{l_2}}\frac{1}{h_{k_d^\star}}+O\Big(h_{n+2}h_{|\mathbf{k}-\mathbf{l}|_1^{s+1,2}}\Big)$$
$$\leq \frac{\mathcal{Q}\|\rho\|_\infty}{Nh_{n+2}}\sum_{\substack{(\mathbf{k},\mathbf{l})^{1,s}\\ \in\mathbb{F}_n^r\times\mathbb{G}_n^{s-r}}}\sum_{\substack{(\mathbf{k},\mathbf{l})^{s+1,2}\in\mathbb{H}_n^{2-s},\\ |\mathbf{l}|_1^{1,2}\leq|\mathbf{k}|_1^{1,2}}}h_{|\mathbf{k}-\mathbf{l}|_1^{s+1,2}}.$$

In addition, for $\mathbf{k},\mathbf{l}\in\mathbb{N}^2$ such that $k_m=l_m$, $m=1,...,r$ and $k_m<l_m$, $m=r+1,...,s$, the following bound is verified, according to Lemma C.5, equation (89):

$$\sum_{\substack{(\mathbf{k},\mathbf{l})^{s+1,2}\in\mathbb{H}_n^{2-s},\\ |\mathbf{l}|_1^{1,2}\leq|\mathbf{k}|_1^{1,2}}}h_{|\mathbf{k}-\mathbf{l}|_1^{s+1,2}}\quad\leq\quad\sum_{\substack{\mathbf{k}^{s+1,2}\in\mathbb{I}_n^{2-s}\\ (\mathbf{l}^{s+1,2})_i\in]\!]1,(\mathbf{k}^{s+1,2})_i-\frac{1}{2-s}|\mathbf{l}-\mathbf{k}|_1^{r+1,s}]\!]}}h_{|\mathbf{k}-\mathbf{l}|_1^{s+1,2}}\quad=\quad\left(2nh_{\frac{|\mathbf{l}-\mathbf{k}|_1^{r+1,s}}{2-s}}\right)^{2-s}$$
$$=(2n)^{2-s}h_{|\mathbf{l}-\mathbf{k}|_1^{r+1,s}},$$

so that using the Lemma C.5, equation (88) and $\mathrm{Card}(\mathbb{F}_0^r) = n^r$ one gets the following bound:

$$\begin{aligned}
&\sum_{\substack{(\mathbf{k},\mathbf{l})\in\mathbb{F}_n^r\times\\ \mathbb{G}_n^{s-r}\times\mathbb{H}_n^{2-s}}} \left|\mathrm{Cov}(\mathcal{I}_{V_{h_{\mathbf{k}^\star}}}\mathcal{V}(\hat{\rho}_{h_{\mathbf{k}^\star}}),\mathcal{I}_{V_{h_{\mathbf{l}^\star}}}\mathcal{V}(\hat{\rho}_{h_{\mathbf{l}^\star}}))\right| \\
&\qquad\leq 2^{2-s}\frac{n^{2-s}\mathcal{Q}\|\rho\|_\infty}{Nh_{n+2}} \sum_{\substack{(\mathbf{k},\mathbf{l})^{1,s}\\ \in\mathbb{F}_n^r\times\mathbb{G}_n^{s-r}}} h_{|\mathbf{l}-\mathbf{k}|_1^{r+1,s}} \\
&\qquad\leq 2^{2-r}\frac{n^{2-r}\mathcal{Q}\|\rho\|_\infty}{Nh_{n+2}} \sum_{\substack{(\mathbf{k},\mathbf{l})^{1,r}\\ \in\mathbb{F}_n^r}} 1 \\
&\qquad\leq 2^{2-r}\frac{n^{2}\mathcal{Q}\|\rho\|_\infty}{Nh_{n+2}},
\end{aligned}$$

II.ii) If $s = 2$: then necessarily $\mathbf{k} = \mathbf{l}$, *i.e.* $r = 2$, and since $\mathrm{Card}(\mathbb{F}_0^r) = n^r$, one gets the following bound:

$$\begin{aligned}
\sum_{(\mathbf{k},\mathbf{l})\in\mathbb{F}_n^2} \left|\mathrm{Cov}(\mathcal{I}_{V_{h_{\mathbf{k}^\star}}}\mathcal{V}(\hat{\rho}_{h_{\mathbf{k}^\star}}),\mathcal{I}_{V_{h_{\mathbf{l}^\star}}}\mathcal{V}(\hat{\rho}_{h_{\mathbf{l}^\star}}))\right| &\leq \frac{\mathcal{Q}\|\rho\|_\infty}{N}\sum_{(\mathbf{k},\mathbf{l})\in\mathbb{F}_n^2}\Big[\frac{1}{h_{k_1}h_{k_2}h_{k_3^\star}} + O\big(h_{k_1}h_{k_2}h_{k_3}^\star\big)\Big] \\
&\leq \frac{n^2\mathcal{Q}\|\rho\|_\infty}{Nh_{n+2}} + O\left(\frac{n^2}{N}\right)
\end{aligned}$$

Finally, combining all the different cases, the following bound is found:

$$\begin{aligned}
\mathbb{V}\left(\mathcal{V}(\hat{\rho}_{h_n}^c)\right) &\leq 36 \sum_{\substack{(\mathbf{k},\mathbf{l})\in(\mathbb{N}^*)^6,\\ |\mathbf{k}|_1=n+2,\\ |\mathbf{l}|_1=n+2,}} \Big[\left|\mathrm{Cov}(\mathcal{I}_{V_{h_{\mathbf{k}}}}\mathcal{V}(\hat{\rho}_{h_{\mathbf{k}}}),\mathcal{I}_{V_{h_{\mathbf{l}}}}\mathcal{V}(\hat{\rho}_{h_{\mathbf{l}}}))\right| + O\left(\frac{1}{N}\right)\Big] \\
&\leq 36(21+4\log(2))\frac{n^2\mathcal{Q}\|\rho\|_\infty}{Nh_n} + O\left(\frac{n^4}{N}\right),
\end{aligned}$$